Final Report

DESIGN OF AN OPTOMETER AND TWO-DIMENSIONAL EYE TRACKER

By T. N. CORNSWEET H. D CRANE

Prepared for:

NATIONAL AERONAUTICS AND SPACE ADMINISTRATION
AMES RESEARCH CENTER
MOFFETT FIELD, CALIFORNIA 94035

CONTRACT NAS2-3517

STANFORD RESEARCH INSTITUTE

MENLO PARK, CALIFORNIA

STANFORD RESEARCH INSTITUTE
MENLO PARK CALIFORNIA

April 1967

Final Report

DESIGN OF AN OPTOMETER AND TWO-DIMENSIONAL EYE TRACKER

By: T. N. CORNSWEET H. D. CRANE

Prepared for:

NATIONAL AERONAUTICS AND SPACE ADMINISTRATION
AMES RESEARCH CENTER
MOFFETT FIELD, CALIFORNIA 94035

CONTRACT NAS2-3517

SRI Project 6009

Approved: F. J. KAMPHOEFNER, MANAGER
ENGINEERING TECHNIQUES LABORATORY

J. D. NOE, EXECUTIVE DIRECTOR
ENGINEERING SCIENCES AND INDUSTRIAL DEVELOPMENT

Copy No. .....

ABSTRACT

A technique for two-dimensional tracking of eye position is described. This technique involves the projection of an infrared pattern into the eye and a measurement of the spatial separation of the first and fourth Purkinje reflections--the reflections from the front of the cornea and back of the lens, respectively. Because the first reflection is from a positive mirror and the fourth from a negative mirror these reflections move in opposite directions under eye rotation, but together under eye translation. By measuring the spatial separation of the two images we therefore obtain a measure of the rotational position of the eye that is not contaminated by artifact from translational movements of the eye. On the basis of preliminary results we have designed an experimental model that should provide tracking over a two-dimensional field at least several degrees in diameter and with an accuracy of 5 minutes of arc or better.

The design of an optometer that gives a continous real-time measure of the total refraction of the eye is also described. In this instrument, an infrared pattern is imaged on the retina and reflected light from the retinal pattern is reimaged externally. By a relatively simple technique, an electronic signal representing the state of defocus of the external image is derived. This signal controls a servo system that maintains the pattern in focus on the retina. As the refractive strength of the eye changes, the effective refractive power of the input system also changes, so as to maintain the input pattern in focus, and the refractive strength of the eye is inferred from the instantaneous refractive power of the input optical system.

CONTENTS

ILLUSTRATIONS

BLANK PAGE

I INTRODUCTION

From a previous study of visual accommodation in humans,[1]* certain hypotheses evolved relating to the size of the retinal region that is involved in focus control, the nature of the signal processing that determines the state of focus, and the nature of the control system. Testing of these hypotheses requires the development of two instruments--a two-dimensional eye tracker and an optometer. The design of two such instruments is discussed in this report.

Though there are a number of devices currently in use for monitoring eye position, none is both accurate and convenient to use. Methods based on the use of contact lenses can provide high accuracy but have obvious inconveniences. Other techniques--e.g., skin-mounted electrodes, or eye-glass-mounted photoelectric pickups--are relatively convenient, but eye position can be measured to no better than 1/2 degree. For the accommodation experiments that we wish to conduct, we require a device with an accuracy of a few minutes of arc over a two-dimensional field of at least a few degrees.

We are presently studying a method of eye tracking that we refer to as the double-Purkinje-image method, a method that requires no attachments to the eye and that seems capable of providing the required accuracy. In Sec. II-A we review some of the currently used eye-tracking devices and describe the new method. Section II-B is an analysis of the new method.

The function of an optometer is to monitor, in real time, the instantaneous refractive strength of the human eye. The basic approach taken here is to image an infrared test pattern onto the retina and to externally reimage the reflected light from the retina. By examining the condition of focus of the external pattern we can infer the condition of focus of the pattern on the retina itself. Defocus signals are used to drive a servo system that maintains the test pattern in focus on the retina at

*References are listed at the end of this report.

all times Changes in eye refraction are measured in terms of the refractive changes required in the input system to maintain the pattern in focus.

In Sec. III-A we consider a basic method of measuring defocus, and in Sec. III-B we consider in some detail the design of an experimental optometer based on this method. The main problem in the design of such an instrument is that the very small amount of light reflected from the retina is easily buried in artifact signals arising from reflections from the other optical surfaces of the eye. The instrument described here is similar in concept to others designed in the past,[2,3] though we have incorporated a change in the optics that permits us to eliminate essentially all of the artifactual signals, and thereby to obtain an instrument with improved performance.

II DOUBLE-PURKINJE-IMAGE EYE TRACKER

A. Review of Eye-Tracking Techniques

1. Contact-Lens Methods

In this class of methods a tightly fitting contact lens is attached to the eye, and either a light source, a mirror, or a coil of wire is attached to the lens. Movements of the eye can then be monitored by electro-optical tracking of photography.

These methods provide excellent resolution and, if the lens fits tightly enough, also permit recording over a very wide range of eye positions. They have the obvious shortcoming, however, that the lens must fit tightly on the eye, producing some discomfort. Further, in order to get a tight fit, either each lens must be individually constructed to fit the particular observer (an expensive and time-consuming operation) or the observer's eye must be anesthetized and the lens attached with suction, a difficult and slightly risky procedure.

2. The Electro-Oculogram

Physiological events within any mammalian eye result in the maintenance of a voltage, the so-called resting potential, between the cornea and the surrounding tissue, such as the forehead. Therefore, if two electrodes are placed, say, one on the skin above and the other below the eyeball, vertical rotations of the eye will result in corresponding changes in the voltage between the electrodes. A recording of such a voltage is called an electro-oculogram. The accuracy of this technique is limited by many factors, such as the slow changes in the resting potential with time of day, state of adaptation, etc. Further, the electrical noise level resulting from stray bioelectric potentials is equivalent to an eye rotation of between 15 and 30 minutes of arc (the angle subtended by the head of a thumb tack about 4 to 8 feet away), limiting the resolution of the technique.

3. Tracking a Feature of the Front of the Eye

When the eye rotates in its socket, the location of any feature of the front of the eye, such as the iris or a blood vessel on the white, moves accordingly. Therefore, photography or electro-optical tracking of such a feature provides a method of recording eye position.

Photography is clearly unusable for real-time, continuous measurement. This technique is useful for recording large movements, but its precision is necessarily limited to about 15 to 30 minutes of arc, for the following reason.

When the eye rotates horizontally, the front of the eye moves horizontally. If the head moves sideways, or the eyeball shifts sideways in its socket, the front of the eye also moves horizontally. Therefore, using these techniques, there is no way to distinguish lateral movements of the eye from rotations. For example, a rotation of one degree moves the front of the eye through 0.2 mm, and is thus indistinguishable from a lateral shift of 0.2 mm. On the other hand, the visual effects of rotation are drastically different from those of translation. If the object being viewed is 2 meters away, a lateral movement of 0.2 mm changes the place being looked at by 0.2 mm, while a rotation of 1 degree (which looks the same to the recording device) changes that place by 35 mm. The farther away the target is, the larger becomes the discrepancy between the effects of lateral and rotational movement. Therefore, when the technique used to record eye movements involves the monitoring of the location of any point on the front of the eye, lateral movements result in artifacts. Since it is impossible to prevent the eye from moving laterally in its socket, the error of these techniques cannot be less than about 15 to 30 minutes of arc (corresponding to lateral shifts of the eye of 0.05 to 0.1 mm).

4. Corneal Reflection Techniques

Some of the light incident on the transparent part of the eye, the cornea, is reflected at the cornea-air interface. The cornea acts as a convex mirror, and therefore a virtual image of any object in front of the eye will be formed just behind the cornea. (This image is usually

called the glint in the eye.) Since the center of rotation of the eyeball is not coincident with the center of curvature of the cornea, rotations of the eyeball result in relative movements of this image, the image of a distant object moving about 0.1 mm for each degree of rotation. The corneal reflection is commonly used as an indicator of eye position simply by photographing or tracking the position of the corneal image of a stationary light source.

This technique is suitable for monitoring large eye movements, but it is subject to error when the eyeball shifts laterally for exactly the same reasons as were explained in the preceding section. Its error, therefore, cannot be less than about 15 to 30 minutes of arc.

To reduce the artifact from translation movements it would be useful to have available two features that move similarly under translation but differently under rotation. The corneal-limbus method described in Quarterly Report 1 was such a method. Here we measured the distance between the variable position of the corneal reflection and the fixed limbus (the junction of the cornea and the white of the eye). Although this method is useful for one-dimensional tracking, it is not easily extendable to two dimensions. For one thing, the eyelids normally cover so much of the limbus as to make direct vertical scanning impossible, and a shallow-angle scan leads to poor vertical accuracy.

5. Double-Purkinje-Image Method

We are presently studying a new method of eye tracking that seems extendable to two-dimensional tracking, with the potential of meeting our accuracy requirements. The method is based on the use of a pair of eye reflections that move similarly under translation but differentially under rotation.

The virtual image formed by the reflected light from the front of the cornea is referred to as the first Purkinje image. A second Purkinje image, formed by reflection from the rear surface of the cornea, is almost exactly coincident with the first Purkinje image. The light that is not reflected from either of these surfaces passes

through the cornea, passing in turn through the aqueous humor and then the lens of the eye. The third Purkinje image, a virtual image formed by light reflected from the front surface of the lens, is much larger and more diffuse than the others and is formed in a plane far removed from the plane of the other images. The fourth Purkinje image is formed by light reflected from the rear surface of the lens, where the lens forms an interface with the vitreous humor that fills the bulk of the eyeball. This rear surface of the lens acts as a concave mirror, forming a real image of the source.

The fourth Purkinje image is almost the same size, and is formed in almost exactly the same plane, as the first Purkinje image, though it is over 100 times less intense. If the eye undergoes translation--e.g., a lateral head movement--both images move together through the same distance and direction as the eye. If the eye rotates, the two images change their separation in space, because the first Purkinje image, formed by a convex mirror, and the fourth Purkinje image, formed by a concave mirror, move in opposite directions with reference to the line of sight of the eye. Referred to a fixed point in space, both images move in the direction of rotation of the eye, but they move by different amounts. The physical separation between these two images in space yields a measure of the angular rotation of the eye in the direction of the shift, and the measure is nominally uncontaminated by lateral movements. For two-dimensional tracking we measure the shift in two orthogonal directions.

The device we are constructing will provide a pair of continuous electrical signals whose magnitudes are proportional to the two orthogonal components of separation between the first and fourth Purkinje images of a source of light. This in effect provides continuous monitoring of the angular position of the eyes, or of the point in space at which the gaze is directed. Since lateral-movement artifacts have been substantially eliminated, the accuracy will be limited primarily by the quantal fluctuations in the very-low-intensity fourth Purkinje image. A more detailed analysis of the system is given in the next section.

B. Analysis of Double-Purkinje-Image Method

1. Outline of the Overall System

Figure 1 is a diagram of the optical system currently being used. Condensing lens L_1 forms an image of the source in the plane of stop ST_1, which is a variable aperture that can be moved vertically and

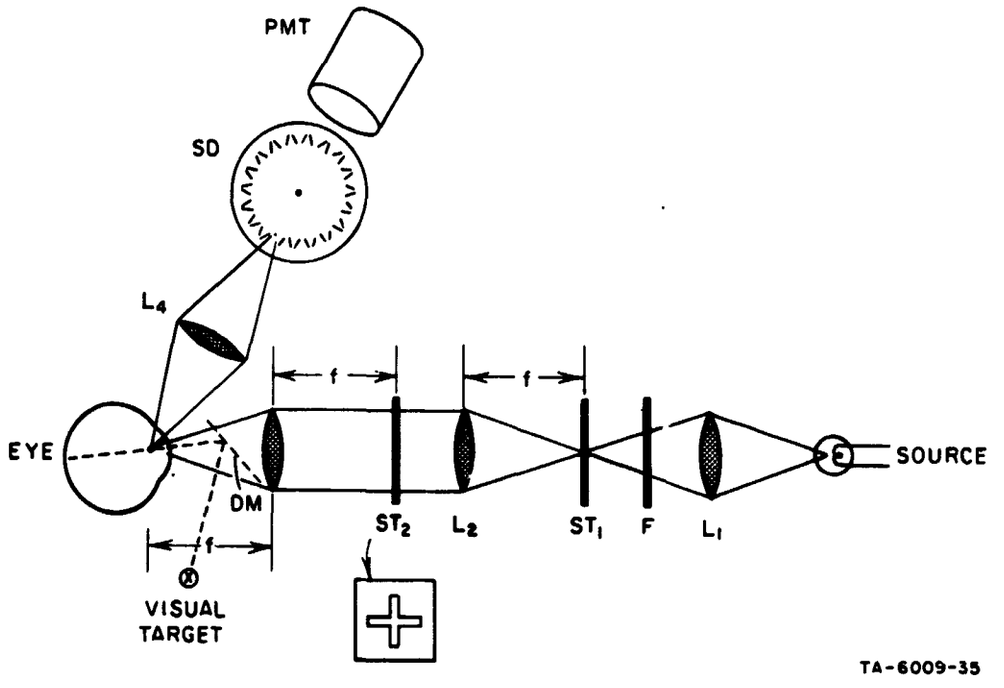

FIG. 1 BASIC OPTICS OF THE EYE TRACKER

horizontally. Lens L_2 collimates the light from ST_1, and filter F passes a band of wavelengths from about 850 to 1050 nanometers. Thus, the measuring light is invisible and does not interfere with visual tasks. The filtered light then passes through stop ST_2, which contain two orthogonal slits. Lens L_3 collimates the light from these slits and images ST_1 in the plane of the pupil of the eye.

The reflected components of the light from the front of the cornea and the rear surface of the lens of the eye form virtual and real images, respectively, of stop ST_2. The light radiating from these images

is imaged by viewing lens L_4 in the plane of a scanning disk, SD, which rotates at about 6000 rpm and contains 90 pairs of orthogonal slits. The two Purkinje images are thus scanned 9000 times per second. Light passing through the slits falls on a photomultiplier tube PMT. The dashed line labeled DM is a dichroic mirror which transmits the infrared measuring light and reflects visible light from the target being viewed.

Figure 2 shows the motion of the disk across the two Purkinje images formed in the plane of the disk. The images are displaced with respect to each other, indicating in this case a general condition where

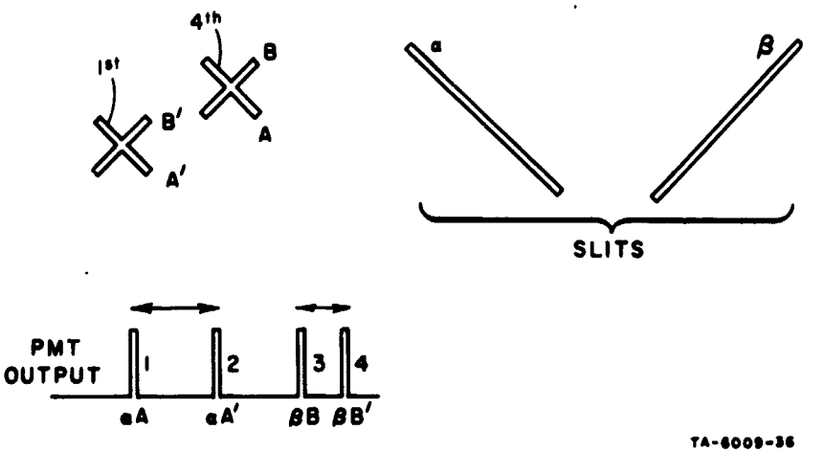

FIG. 2 PHOTOCELL SIGNALS FROM WHICH EYE POSITION IS DETERMINED

the eye is pointing upward and to the right of an arbitrary reference position at which, say, the two cross points of the images would coincide. As the disk rotates, light will strike the photomultiplier as slit α crosses line A and then line A′, and then as slit β crosses line B and then B′. The time between Pulses 1 and 2 is a measure of the component of eye position in the direction perpendicular to lines A and A′, and the time between Pulses 3 and 4 is the component perpendicular to lines B and B′. Signals representing the magnitude of these time intervals are the final outputs of the instrument.

2. Relevant Eye Dimensions

In the remainder of this section we will try to analyze the way in which the Purkinje images move in space under eye rotation. For this purpose a knowledge of certain of the eye dimensions is important. There is great variation from eye to eye, but the values in Fig. 3 are typical.

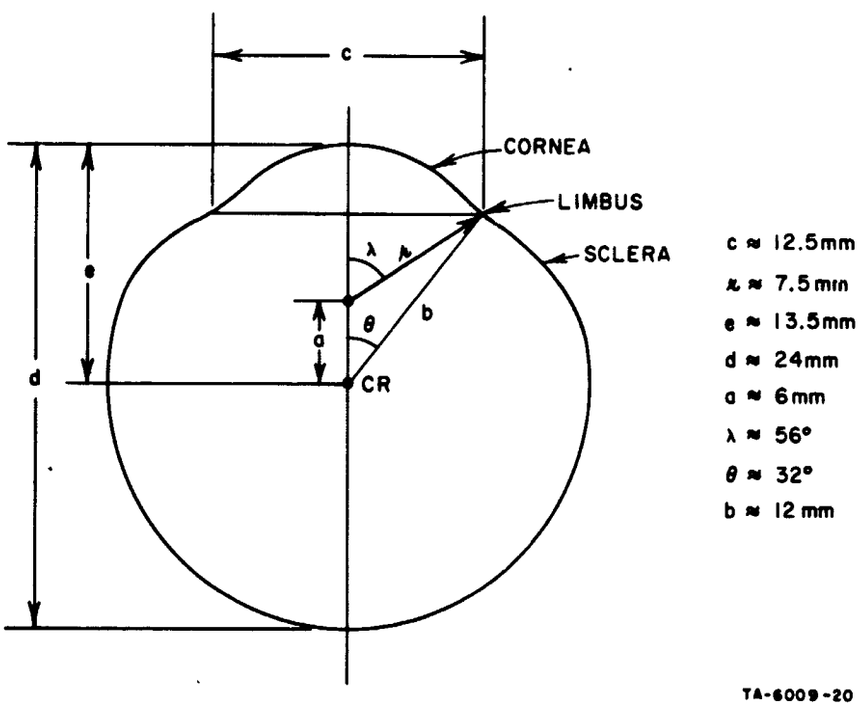

FIG. 3 RELEVANT EYE DIMENSIONS

The overall globe is a somewhat flattened sphere, as shown in the figure. The transparent cornea has a radius of curvature r $\approx$ 7.5 mm, with the center of curvature (C) displaced by a distance a $\approx$ 6 mm from the center of rotation (CR) of the eye, which is located about 13.5 mm from the front of the cornea. The cornea merges with the sclera (or "white of the eye") at a region called the limbus, which forms a ring (around the edge of the cornea) of diameter c $\approx$ 12.5 mm. Viewed from the center of curvature of the cornea, the subtended arc of the limbus is $2\lambda \approx 112°$.

3. Position of the Purkinje Images

The reflection coefficient at the interface of two transparent dielectric materials is

$$R = \left(\frac{n_1 - n_2}{n_1 + n_2} \right)^2 \tag{1}$$

where n_1 and n_2 are the indices of refraction. In the case of the air-cornea interface, the reflection coefficient is

$$R = \left(\frac{1.376 - 1}{1.376 + 1} \right)^2 = 0.025 \tag{2}$$

where 1.376 is the index of refraction of the corneal material. In other words, approximately 2.5 percent of the incident light is reflected by the cornea, and is contained in the first Purkinje image.

To find the form of the reflected image, consider a distant light source reflected in the positive (i.e, convex) mirror of Fig. 4.

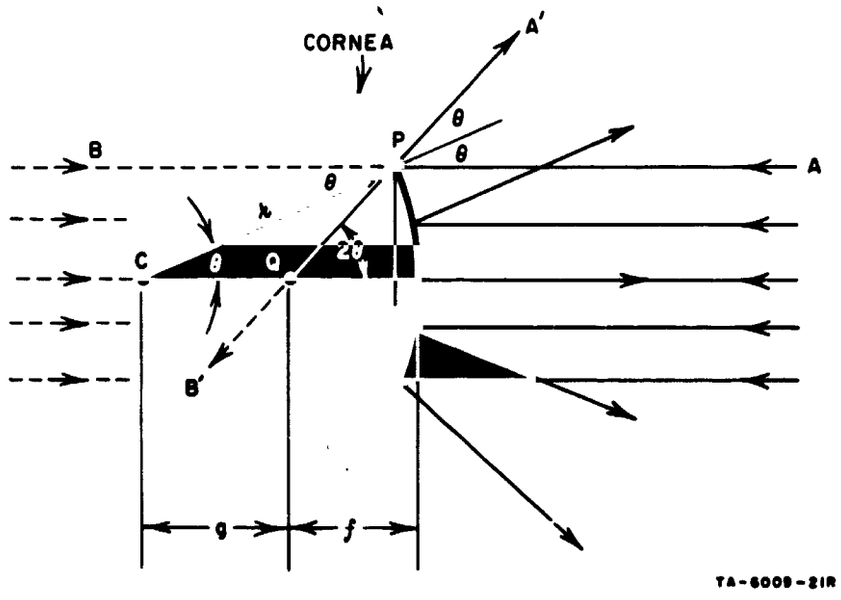

FIG. 4 REFLECTION OF A DISTANT SOURCE IN A POSITIVE AND NEGATIVE MIRROR

(Neglect for the moment the incoming rays from the left.) The input ray A makes an angle θ with the radius drawn to the intercept point P. The reflected ray A′ similarly makes an angle θ with the radius; and if this reflected ray is extended backwards, it intersects at an angle 2θ the ray parallel to A and drawn through the center of curvature C. The intersection point will be at a distance f from the front of the mirror, where

$$f = r\,(1 - \cos\theta) + \frac{r(\sin\theta)}{\tan 2\theta}$$

$$= r\left[1 - \frac{1}{2(\cos\theta)}\right] \qquad (3)$$

or a distance g from the center of curvature, where

$$g = r - f = \frac{r}{2(\cos\theta)} \quad . \qquad (4)$$

For small θ we have $f \approx r/2$, which is the well known focal length for a mirror, and represents the image plane for a distant object.

The fourth Purkinje image is formed by light reflected from the rear surface of the lens, that passes back out through the cornea. An equivalent single mirror that would form the same external image is shown by the heavy line in Fig. 5(a). The radius of this mirror is about 5.8 mm (compared with the corneal radius of 7.8 mm) and its center is close to the corneal surface.[4] The curvature and position of the equivalent mirror shifts with changes of accommodation. For an 8.6 diopter change (which is a very large change in accommodation), the mirror changes, as shown, to 5.2 mm radius with its center shifted slightly further from the corneal surface.

Ray-tracing with a negative (concave) mirror is similar to that with a positive mirror. The same mirror of Fig. 4 serves as a negative lens for the dashed rays impinging from the left. In particular, Ray B, which is along the same line as Ray A, is reflected as Ray B′, which is along the same line as Ray A′ and we see then that

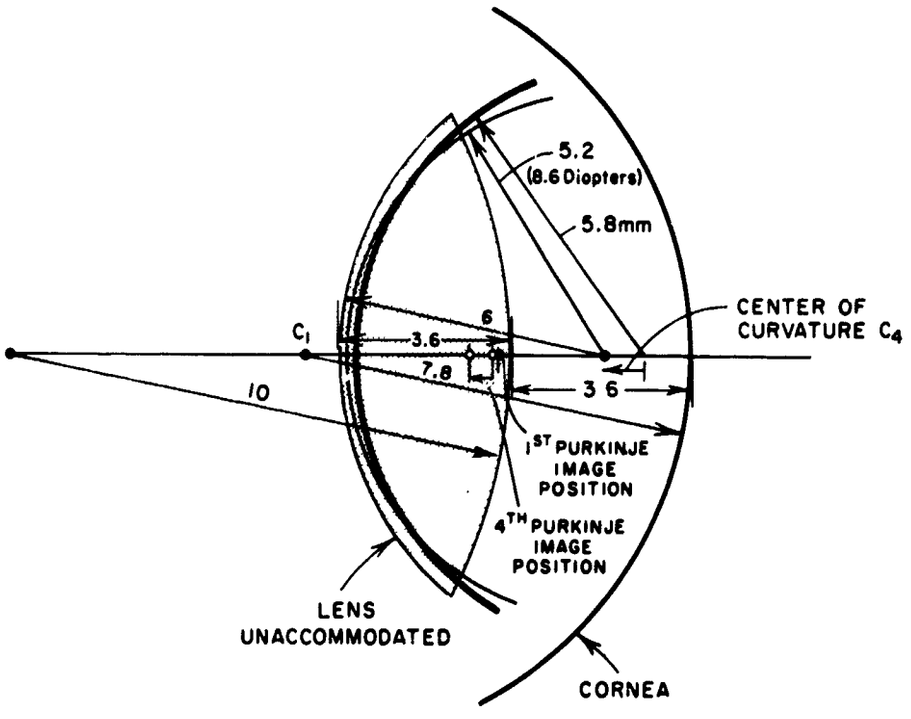

(a)

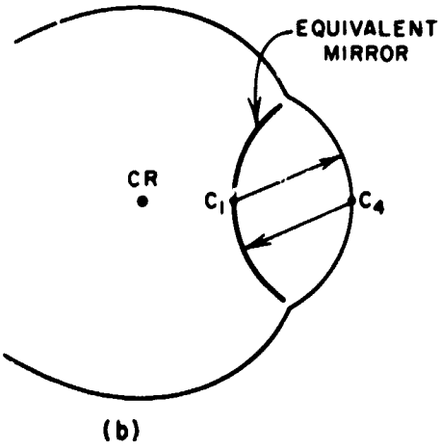

(b)

TA-6009-37

FIG. 5 OPTICS OF PURKINJE IMAGE FORMATION

(a) Position of equivalent fourth Purkinje mirror for unaccomodated eye and eye accomodated by 8.6 diopters

(h) assuming, for simplicity, that the first Purkinje mirror (cornea) and equivalent fourth Purkinje mirror form a symmetrical "clamshell"

exactly the same Eqs. (3) and (4) apply for the negative mirror as well. The position of the (virtual) corneal image plane is shown by the solid dot (on the axis) in Fig. 5(a). The position of the fourth Purkinje image is shown by the open dot, and we see that in the unaccommodated condition the planes of the first and fourth images are almost identical.

We will eventually have to concern ourselves with the effects of accommodation change, which the optometer will be simultaneously monitoring. But to greatly simplify the analysis here let us simply assume that the equivalent mirror for the fourth Purkinje image has the same curvature as the cornea, and that they are separated exactly by their radius of curvature, as shown in Fig. 5(b), where C_1 is the center of curvature for the cornea (first Purkinje image) and C_4 is the center of curvature for the fourth Purkinje image.

It is important to note that the real image from the negative mirror is inverted with respect to the virtual image from the positive mirror. Thus, as the source moves vertically upward, the virtual image in Fig. 6(a) similarly moves upward, but the real image of Fig. 6(b) moves downward. This is the differential separation, with rotations, in which we are interested.

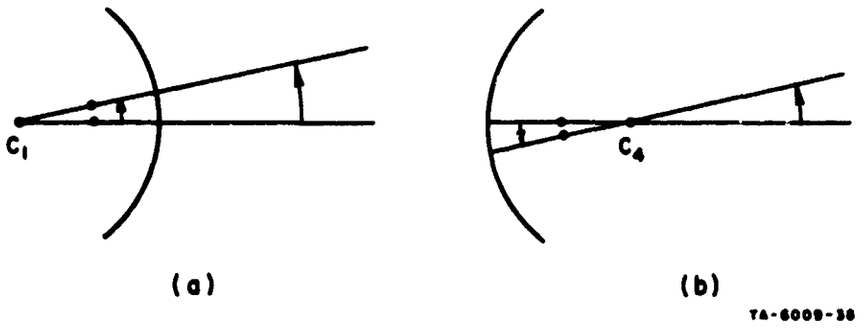

FIG. 6 ILLUSTRATION OF IMAGE MOVEMENT IN OPPOSITE DIRECTIONS FROM A POSITIVE AND NEGATIVE MIRROR

Another effect that we will have to consider further is the effect of pupil size on the fourth Purkinje image. The light contained in the corneal reflection is reflected from the surface of the cornea and never actually enters the eye. But light from the fourth image must pass the pupil twice, and changes in pupil size can have a significant effect on the intensity and extent of the fourth image.

4. Form of the Purkinje Images

Using the optical arrangement of Fig. 1, consider a line object in the focal plane of lens L_3, Fig. 7. From each point of the line is a fan of rays with an angular spread that depends on the size of the stop

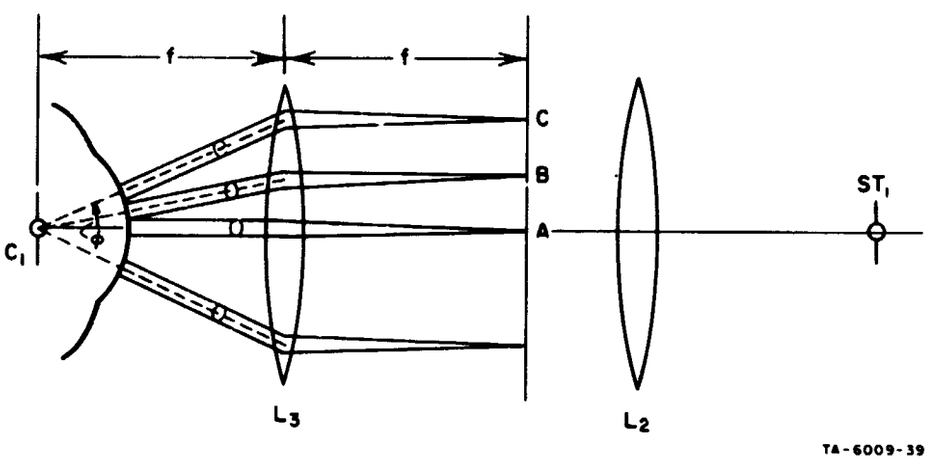

FIG. 7 INPUT RAY CONFIGURATION WITH STOP ST_1 IMAGED AT THE CENTER OF CURVATURE OF THE CORNEA

ST_1. (Only a few fans are shown in the figure.) Each fan is collimated by Lens L_3 and all come together at the image of ST_1. It is assumed in Fig. 7 that the image of ST_1 falls on the center of curvature of the cornea. Let us consider the image of the line that is formed under these circumstances.

In Fig. 8 is an enlargement of the rays impinging on the cornea. Consider the horizontal circular bundle, and assume that it is broken up into separate circular zones. Because the g-distance, in terms of Fig. 4, varies with angular intercept, we see that the "image point" will be different for each circular zone of the input beam. The rays

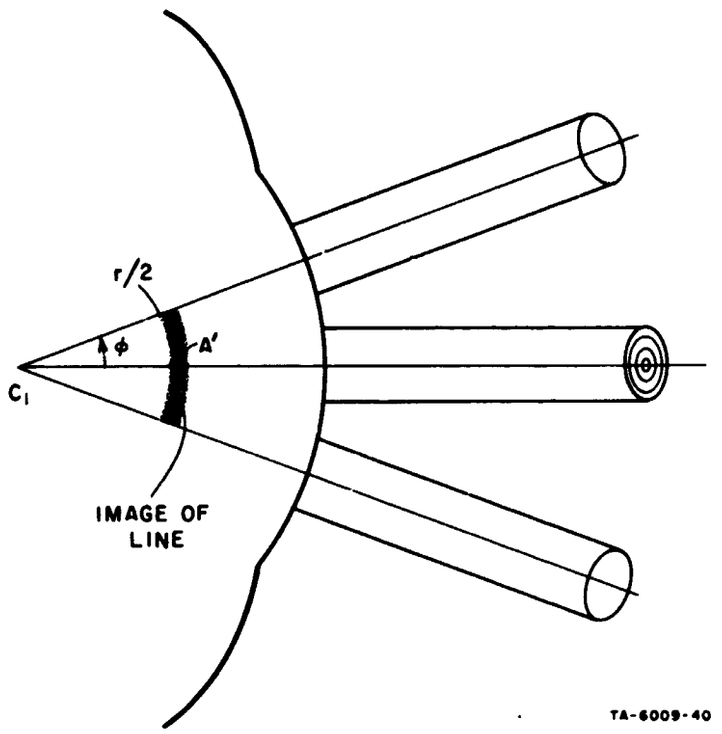

FIG. 8 SPHERICAL ABERRATION EFFECTS
IN A SPHERICAL MIRROR

close to the axis reflect as though from a point at a distance of half the radius (i.e., g = r/2), but g increases for rays further removed from the axis. Thus, the image A′ of the point A on the input line is smeared along the horizontal axis, from a distance r/2 outward to a distance that depends on the radius of the input beam and therefore on the size of the stop ST_1. Exactly the same considerations hold for each point of the line object, so it is clear that the total image of the line will be curved along the r/2 circle, as shown in Fig. 8, with an outward radial spread that depends on the input stop size.

Thus far we have assumed that the stop was made to image on the center of curvature of the cornea, and in this case we see that the corneal image (or first Purkinje image) of the line-object is basically a curved segment along the r/2 circle. But with this optical arrangement, the fourth Purkinje image would be quite different, since the input rays

would be converging, under the assumption of Fig. 5(b), not on the center of curvature for the concave mirror, but directly on the mirror surface itself. If we move the eye back, to the left in Fig. 7, so that the input rays converge on the corneal surface, then the situation would be reversed. The rays would now be converging on the center of curvature for the fourth image and directly on the mirror surface for the first image. To achieve symmetrical image formation of the first and fourth images the image of the stop must fall half-way between the two mirrors, almost exactly in the plane of the natural pupil.

Let us consider the effect on the image of different axial positions of the eye. Assume that the image of the stop is made to fall directly on the corneal surface, as suggested by the single input bundle of Fig. 9. The central ray M will reflect as though from a point distant $g = r/2 \cos\theta$ along a line N drawn through the center of curvature and and parallel to M. To find the reflection centers for all of the other rays in the input beam it is convenient to again consider circular zones, but this time around line N. The sectors closer to N (e.g., zone a) will reflect as though from a smaller g-distance, and those further from N (e.g., zone b) will have a larger g-distance. Thus, the "image" will spread along N, from Point A to Point B, which represents the extreme g-distances. For a circular stop ST_1, so that the input beam from each point of the line object is circular, there will be a large concentration of rays at the central point M, the concentration reducing to zero at the extremes A and B. There will also be a moderate concentration of rays (cross-hatched region in Fig. 9) along a line drawn between the region of concentration along the radial line, and the region where the input beam intersects the corneal surface.

If we consider all of the input rays, the image has the form shown in Fig. 10(a)--primarily a vertical line with a spread that increases with angular position in the incoming beam. The locus of M points is exactly a vertical line, since the g-distance for each M point is $(r/2) \cos\theta$, which has a horizontal component r/2--i.e., independent of θ. The locus of the second concentration of rays falls along

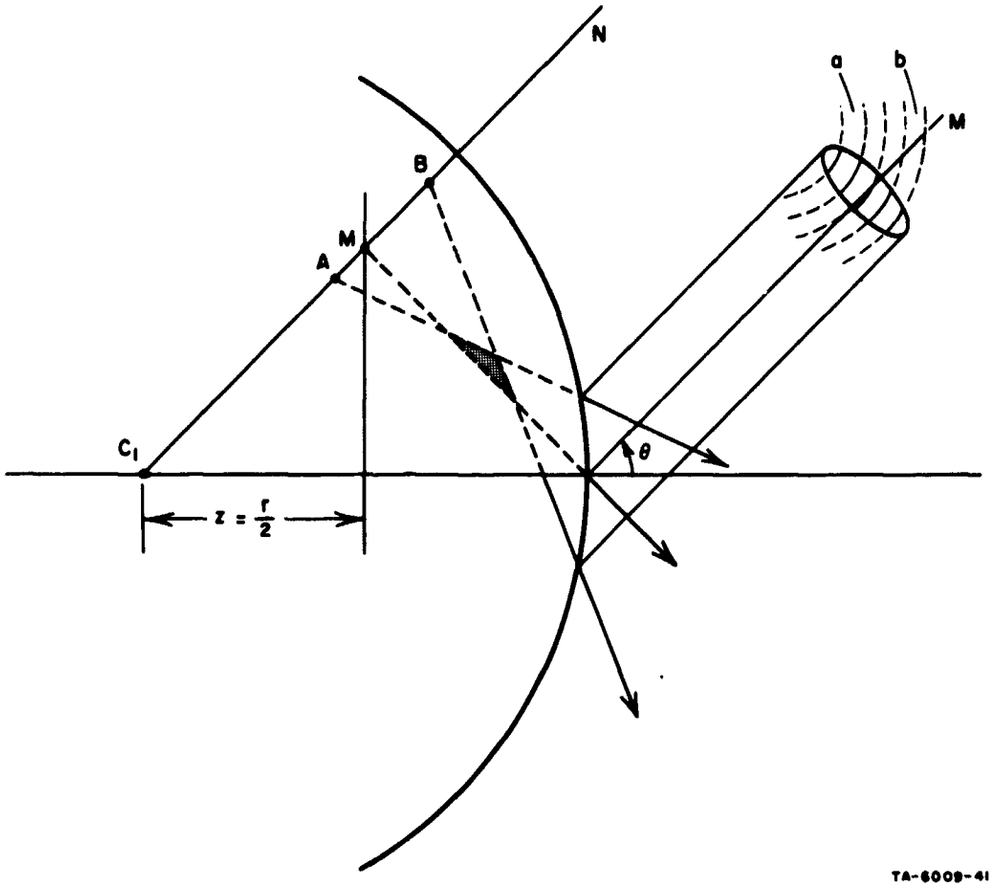

FIG. 9 IMAGE FORMATION WHEN THE INPUT STOP ST_1 IS IMAGED DIRECTLY ON THE CORNEAL SURFACE

the dashed line in the figure. Thus, the primary image is basically a vertical line segment with radial smear.

If we shift the eye so that the stop is imaged in the r/2 plane, as in Fig. 10(b), then the image, as would be expected, falls between the r/2 circular segment of Fig. 8, and the vertical image of Fig. 10(a).

Thus, we see that the form of the corneal image changes with axial eye position, from basically a vertical image when the input stop is imaged on the corneal surface to a segment of the r/2 circle when the stop is imaged in the plane of the center of curvature. It is readily demonstrated that the considerations are the same for the fourth Purkinje

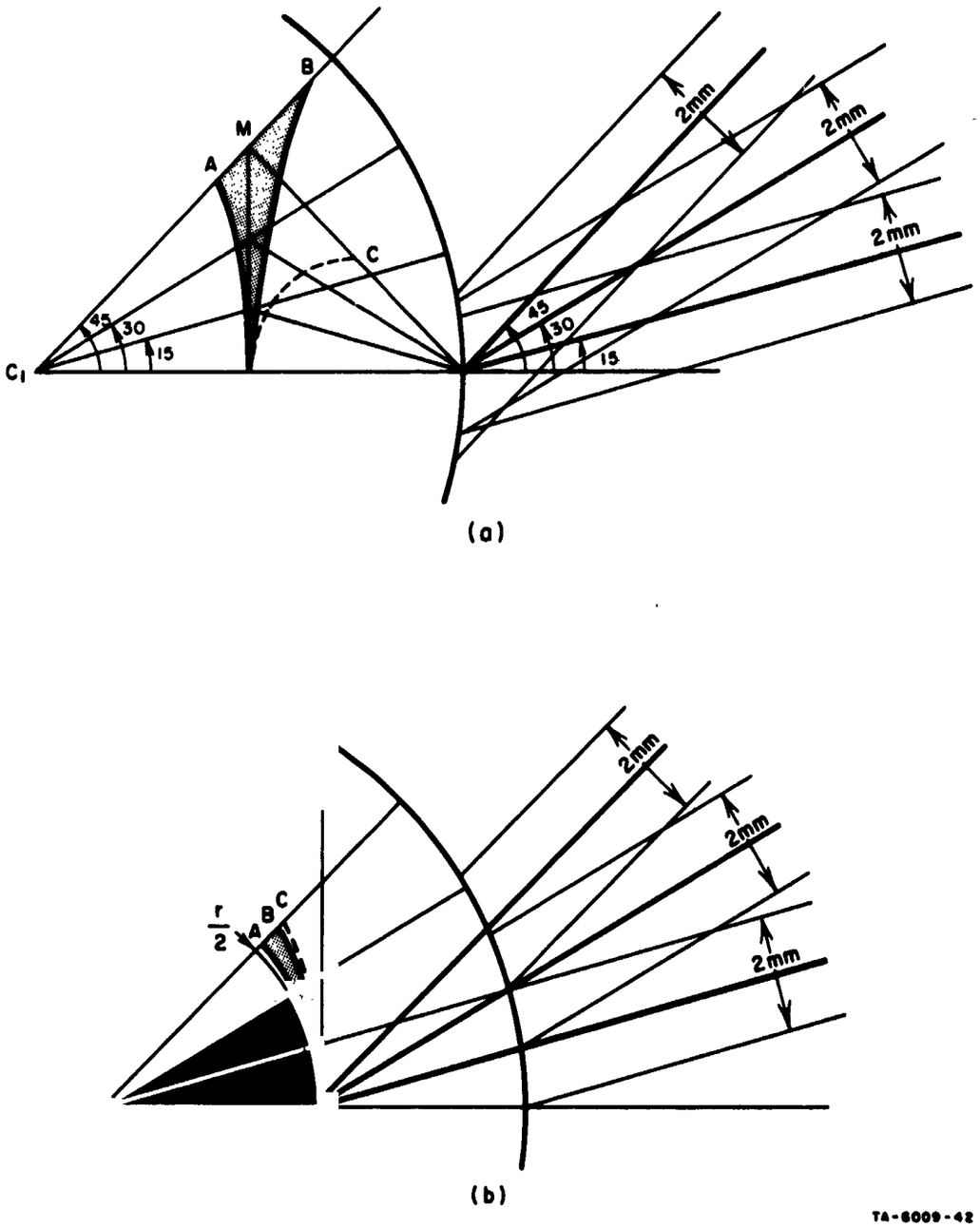

FIG. 10 FORM OF THE CORNEAL IMAGE WITH THE INPUT STOP IMAGED IN (a) THE SURFACE OF THE CORNEA, AND (b) THE r/2 PLANE

image except that the image is inverted. In the final apparatus we will scan both images with the same set of slits and we therefore desire both images to have nominally the same shape. For this reason we attempt to image the stop at the r/2 plane, in which position the two images are tangent back-to-back, as in Fig. 11 (though recall that the first image is virtual and the fourth image is real).

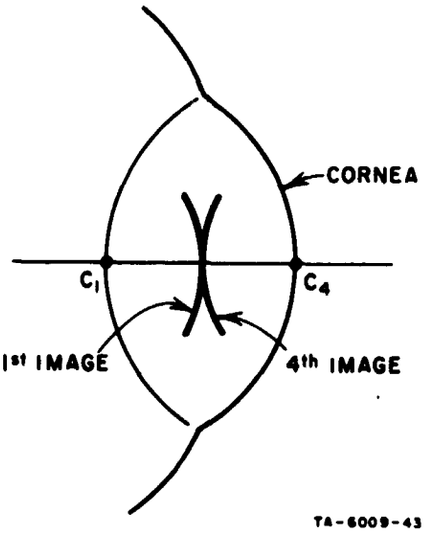

FIG. 11 FIRST AND FOURTH PURKINJE IMAGES OF LINE OBJECT WITH THE INPUT STOP IMAGED IN THE r/2 PLANE

We now have a rough idea of the form of the Purkinje images. Our main interest, however, is how these images move in space, as a function of eye rotation, since it is the differential movement of the two images which, in effect, we use to measure the magnitude and direction of the eye rotation. In the following section we will consider the nature of these image movements with eye rotation.

5. Image Movement with Eye Rotation

The result of an eye translation parallel to the line object is sketched in Fig. 12(a), where only the central ray S and extreme rays R and T are labeled. (This assumes a pinhole stop ST_1 so that in effect there is only a single ray from each point of the line object.) The

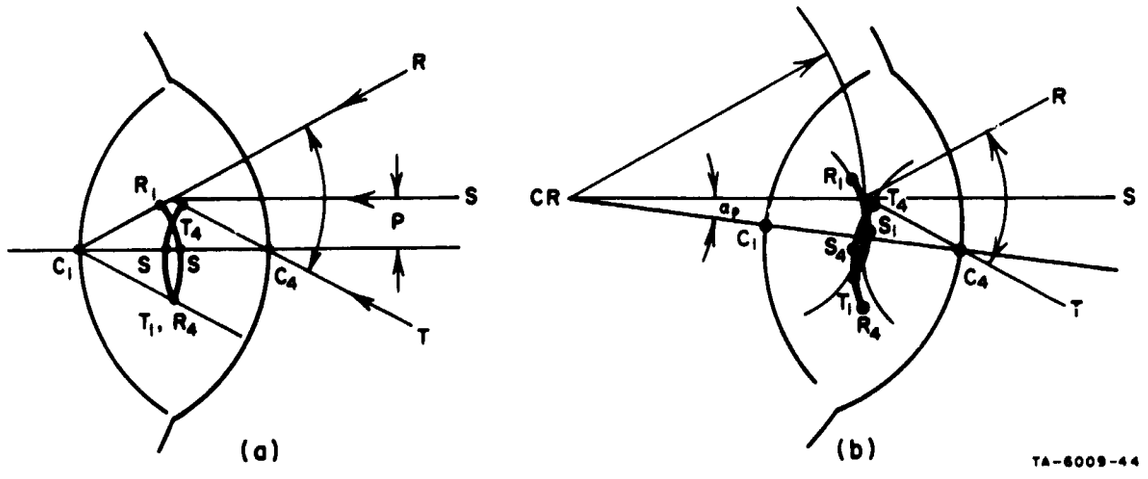

FIG. 12 IMAGE SHIFT WITH (a) EYE TRANSLATION PARALLEL TO THE LINE OBJECT, AND (b) EYE ROTATION PARALLEL TO THE LINE OBJECT

magnitude of translation, P, was chosen so that the extreme rays pass through the centers of curvature. In this case Ray R passes through C_1, the center for the first Purkinje image (corneal reflection), and the corresponding image point is directly on the r/2 circle around C_1, as indicated by Point R_1. Similarly, Ray T passes through center C_4, and the corresponding image point T_4 in the fourth Purkinje image is on the r/2 circle around C_4. Horizontal ray S images along the horizontal line through the centers C_1 and C_4, though the corresponding g-distances are now larger than r/2, and the two images actually cross in space as shown.

If the eye rotates parallel to the line object (i.e., along the line object), rather than translating parallel to the line, then the two images not only cross in space but are differentially displaced vertically. In Fig. 12(b) the rotation angle, α_p, was chosen so that the lower ray T just passes through center C_4. The center for eye rotation is labeled CR. The form of the images in this case is clear from Fig. 12(b).

Though the images of the line object are generally curved in space, they are curved in the plane containing the object and image. Viewing directly into the eye the images would therefore appear straight, and superimposed, although with eye rotation they would be displaced vertically. If these images were swept past a single long slit, the two images would pass the slit simultaneously. In other words, the recording instrument would not be sensitive to either translational or rotational movements parallel to the line.

Let us next treat movements transverse to the line object. Consider a transverse rotation α_T about the center of rotation CR (Fig. 13)

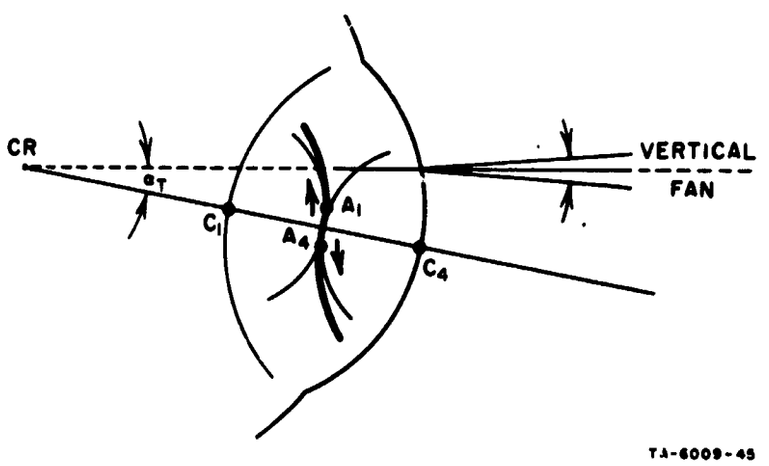

FIG. 13 IMAGE SHIFT WITH EYE ROTATION TRANSVERSE TO THE LINE OBJECT

We assume that the input fan is perpendicular to the page (suggested by the very thin fan shown). This means that the two Purkinje images are nominally perpendicular to the page. To find how these images separate with angular rotation, let us consider only the central (horizontal) ray of the input fan. For the angular rotation angle shown, the first image will form at A_1--i.e., the vertical (curved) line in space penetrates the page through point A_1--and the fourth image will form at A_4. Both images will be beyond the r/2 distance, though the g-distance will be larger for the fourth than for the first image. In any case, we see that

the line images separate in space by an amount nominally proportional to the angular rotation of the eye, and in a plane nominally perpendicular to the optical axis. The exact shape of the (curved) line images will change slightly with rotation (we have only considered the locus of the center point). Note that the images move in different directions only in "eye space." In real space both images move in the same direction, but differentially.

6. Viewing System

We must consider now how to view and image these Purkinje reflections and measure their separation, which is our desired measure of eye rotation.

If the incoming fan is imaged at the center of curvature, then the reflected fan is coincident with the incoming fan, in space, each ray being reflected on itself--e.g., Ray a reflected as Ray a', in Fig. 14(a). If the incoming fan is imaged at the surface of the cornea, the

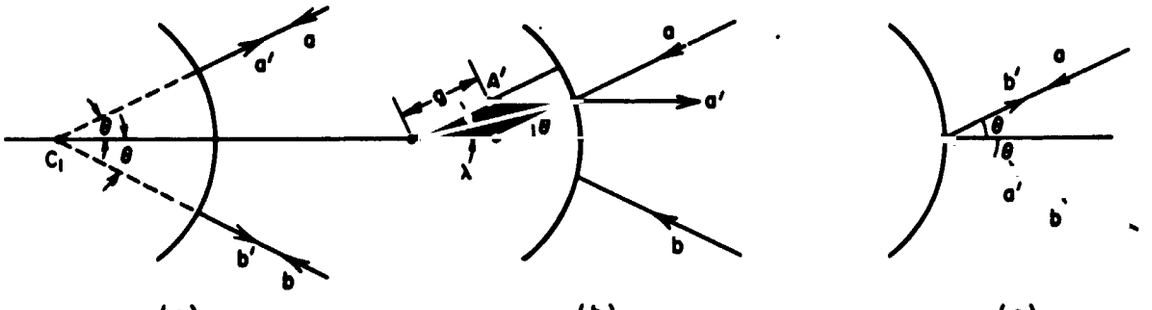

FIG. 14 FORM OF THE REFLECTED BEAM FOR THE INPUT STOP ST_1 IMAGED AT (a) THE CENTER OF CURVATURE, (b) THE r/2 PLANE, AND (c) THE SURFACE OF THE MIRROR

returned beam again has the same shape, but inverted as in Fig. 14(c). With the fan imaged at r/2, which is the focal length of the mirror, the returned beam is nominally collimated [Fig. 14(b)]. This assumes a pin-hole stop ST_1, so that there is essentially only a single ray for each object point. As the stop size increases, each input ray becomes a parallel bundle of rays and the reflected bundle of rays becomes larger in space, and a larger collecting system is therefore required. We will

treat these points further, but first let us consider the general form of viewing system that we might use.

In Fig. 15 we show the arrangement for projecting a given pattern to the eye, in conjunction with an artificial pupil stop, which is shown imaged in the r/2 plane. There are basically two techniques for viewing the resulting Purkinje images. In one case we use a beam

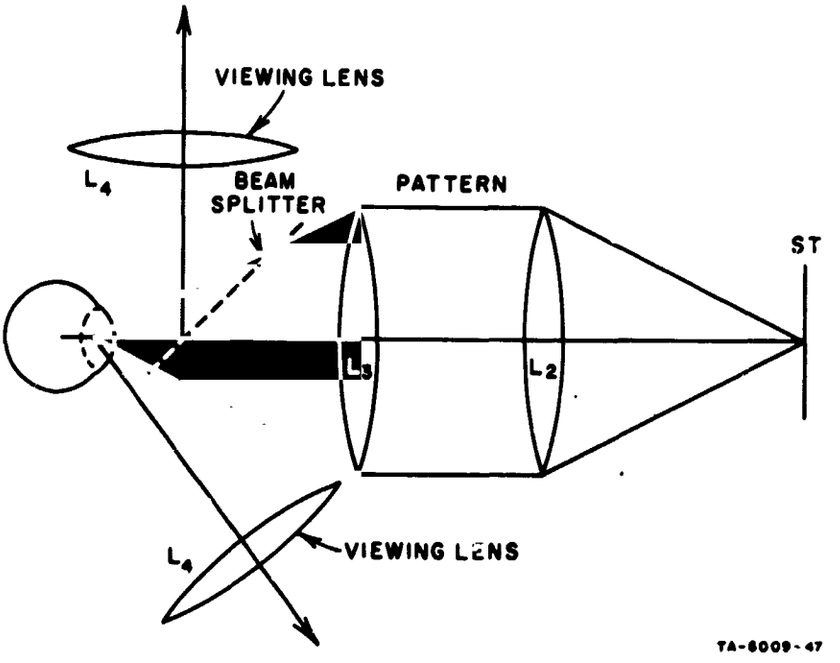

FIG. 15 TWO POSSIBLE ARRANGEMENTS FOR THE VIEWING LENS L_4

splitter and place the viewing lens L_4 off to the side. In the other arrangement we view directly from an angle. An advantage of the latter technique is that we do not have the four-fold loss of light that we have with a beam splitter (a factor of 1/2 in each direction). On the other hand we may have more image distortion to contend with if we view the curved images from off-axis, and also we must consider the difficulty of placing the viewing lens sufficiently close to the eye without interfering with the eye-piece lens L_3. We see then that there are many design questions to consider. Perhaps the most important at the moment though, is the question of field of view.

With the input stop imaged in the r/2 plane, consider what happens to the reflected beam as the eye rotates. As a first approximation we can expect that the collimated return beam of Fig. 14(b) will simply rotate, and remain substantially collimated. To determine just how much the return beam swings in space, we will consider what happens to the central incoming Ray a, in Fig. 16. If the eye rotates by an amount α,

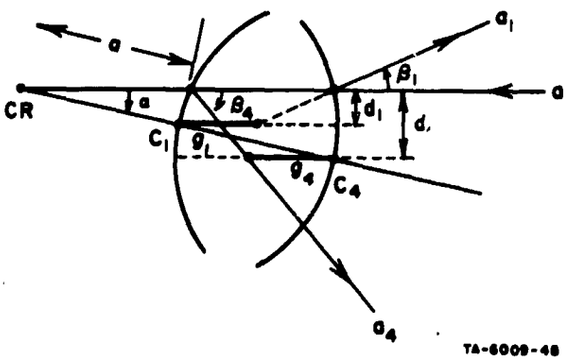

FIG. 16 ANGULAR SWINGS β_1 AND β_4 OF THE COLLIMATED RETURNED BEAMS, FOR AN EYE ROTATION α

about CR (the center of rotation of the eye), then Ray a is displaced by $d_1 = a\alpha$ (assuming small angles) and, in terms of Eq. (4), we have an imaging factor

$$g_1 = \frac{r}{2\cos\theta} \tag{5}$$

where

$$\theta \approx \frac{d_1}{r} \tag{6}$$

or

$$g_1 \approx \frac{r}{2}\left[1 + 1/2\left(\frac{d_1}{r}\right)^2\right] \quad . \tag{7}$$

This leads to a reflection angle β_1, where

$$\beta_1 \approx \frac{d_1}{r - g_1} \tag{8}$$

$$\approx 2\left(\frac{a}{r}\right)\alpha \quad . \tag{9}$$

In other words, if the eye rotates down by 1 degree, the reflected ray swings up by 1.6 degrees, since from Fig. 3 we see that $a/r = 0.8$.

As for the fourth Purkinje reflection we note that the parallel ray, drawn through the center of curvature C_4, is displaced by $d_4 = (a + r)\alpha$. We can calculate the deflection angle β_4 by rewriting Eqs. (5) through (9) with d_4 substituted for d_1, with the result

$$\beta_4 \approx 2\left(\frac{a + r}{r}\right)\alpha = 3.6\ \alpha \tag{10}$$

That is, the deflection angle is about 3.6 times the eye rotation.

We see then that if the eye rotates by α, the two collimated return beams--from the first and fourth images--swing in opposite directions by an amount 1.6 α and 3.6 α, respectively. If a viewing lens L_4 is placed so that the images are near its focal plane (Fig. 17), the effective viewing angle of the lens must be at least twice 3.6 α, or 7.2 α. Thus, for an f/1 lens [which has a focal-length-to-diameter ratio of unity, and therefore a field $\theta = 2\ \tan^{-1}(1/2)$, or 53 degrees] the very largest eye movement away from the axis that we could permit, without losing the fourth image, is (53/7.2), or about 7 degrees. With an f/2 lens, with a field of 28 degrees, the corresponding largest eye movement allowed is only 4 degrees.

These large swings of the reflected beams make it difficult to achieve a large field of view, and any techniques for enlarging the field of view are therefore important. We will see in the next section that the field of view is increased simply by increasing the size of the artificial pupil, and in Sec. 8 we will achieve an even larger increase

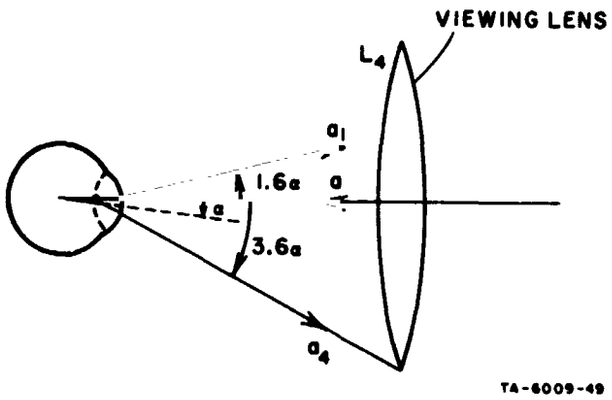

FIG. 17 REQUIRED FIELD OF VIEW OF THE VIEWING LENS L_4

in field of view by having the pupil stop ST_1 move laterally, so as to track the eye movement.

7. Enlarging the Artificial Pupil

Suppose that we open the stop ST_1 so that its image has a diameter 2W at the eye. Now, each ray of the previous input fans is replaced by a parallel beam of diameter 2W. The on-axis beam in Fig. 18(a) is reflected as a spreading beam of angular width 2β. To find β we compute the angle of reflection for the uppermost ray of the input beam, which is displaced a distance W from the optic axis. The horizontal distance from the intersection point at the mirror surface to the center of the mirror is $x = \sqrt{r^2 - W^2}$, so that we have

$$\tan\beta = \frac{W}{x - g} \tag{11}$$

where

$$g = \frac{r}{2\cos\lambda}$$
$$\sin\lambda = \frac{W}{r} \tag{12}$$

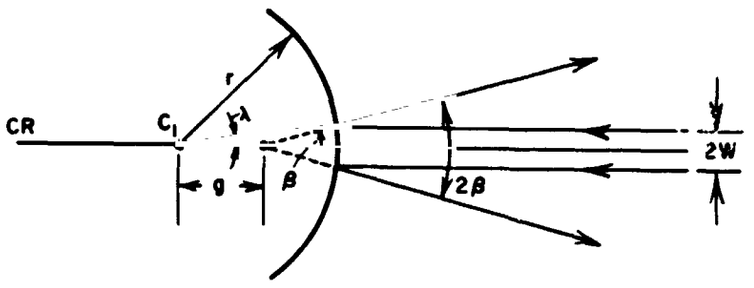

(a)

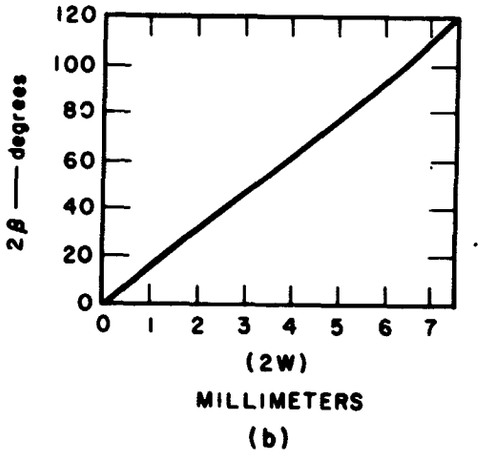

(b)

TA-6009-50

FIG. 18 RELATION BETWEEN THE INPUT BEAM WIDTH AND THE ANGULAR SPREAD OF THE RETURN BEAM

or

$$\tan\beta = \frac{2\sqrt{\left(\frac{r}{W}\right)^2 - 1}}{\left(\frac{r}{W}\right)^2 - 2} \qquad (13)$$

which is plotted in Fig. 18(b), and from which we see a quite linear relation between (2β) and (2W)

As the input beamwidth increases we get a corresponding increase in reflected angular beamwidth, and increase in field of view, although the intensity of the final image will not be the same over the field. As the eye rotates, the reflected beam in Fig. 18(a) will similarily rotate and be swept across the fixed viewing lens. Consider, for example, an f/2 lens with an angular field of 28 degrees and a beamwidth of $2W \approx 1.8$ mm, which from Fig. 18(b) also leads to an angular beamwidth of 28 degrees. With the eye on-axis, the entire returned beam is captured by the viewing lens. As the eye rotates, less and less of the beam is captured by the lens, and the intensity of that particular image point will decrease. In fact, even with the eye fixed on-axis the image will have nonuniform intensity since input beams (of the same width 2W) but representing off-axis points of the line object--and therefore skewed with respect to the optic axis--will have substantially the same angular magnitude of reflected beams, but skewed so that only portions of the beam are intercepted by the lens.

The larger the input beamwidth 2W, the larger the field of view, but also the larger the spherical aberration, in terms of Fig. 8. If we arbitrarily decide that the distance factor $g = r/(2\cos\lambda)$ should not vary by more than say 5 percent from the edge to the center of the beam, or $\cos\lambda = 0.95$, then from Eq. (12) we have

$$\cos\lambda = \sqrt{1 - \sin^2\lambda} = \sqrt{1 - \left(\frac{W}{r}\right)^2} = .95 \qquad (14)$$

or a beamwidth $2W \approx 4.5$ millimeters, which from Fig. 18(b) implies an output angular beam of about 70 degrees. This represents a respectable increase in field but without a great increase in spherical aberration.

Because of constraints imposed by the real pupil of the eye, we would not want to increase the input beamwidth much beyond 4.5 millimeters in any case, and generally the beamwidth will be considerably less.

8. Real-Time Tracking by the Artificial Pupil

We saw that the reflected beams can rotate through wide angles in space, as a result of eye rotation, and that this leads to a limit on

field of view because of the limited angular field of the viewing lens. Increasing the size of the artificial pupil increased the angular spread of the reflected beams, and led to some increase in field of view. Another method of increasing the field of view is to use the signals from the eye tracker to move, or servo, the artificial pupil in such a manner that the reflected beams remain relatively fixed in space, or at least so that the swings are significantly reduced.

The basic idea can be seen in Fig. 19, which is the same as Fig. 16 except that the input fan has been translated in the direction

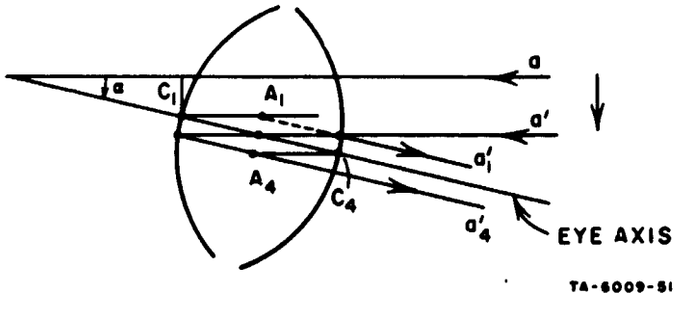

FIG. 19 TRANSLATING THE INPUT STOP ST_1 SO AS TO TRACK THE EYE MOVEMENT

of the eye rotation--i.e., downward--so that the original horizontal ray a, which is now labeled a′, bisects the optical axis between the two centers of curvature. The reflected rays, which are labeled a_1' and a_4', are now nominally parallel to each other and parallel to the eye axis. In other words, if the input aperture tracks the eye rotation in this manner, the returned rays in both Purkinje images, from a given object point, remain parallel to the optic axis, though their separation increases with rotation angle. In this way we cut down the swings of 1.6 α and 3.6 α in Fig. 17 to swings that simply track the rotation itself.

It is important to understand that although movement of the artificial pupil image affects the angles of the reflected beams, it has no effect (at least no first-order effect) on the position of the

Purkinje images themselves. To see that this is so, assume in Fig. 20 that the stop ST_1 is a position A, in the focal plane of lens L_2, and

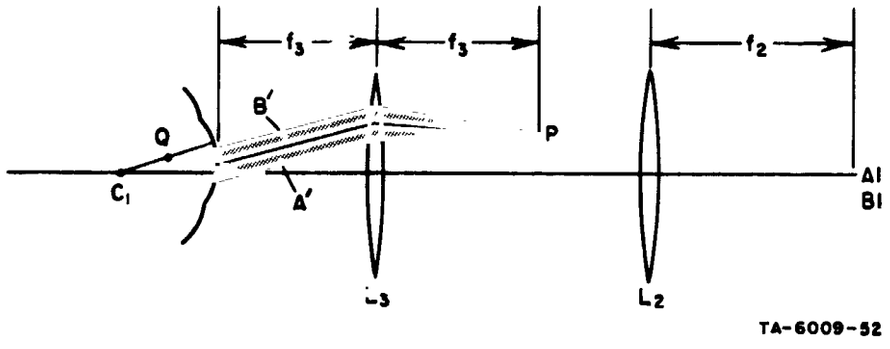

FIG. 20 DEMONSTRATION THAT TRANSLATION OF THE INPUT STOP ST_1 DOES NOT AFFECT THE POSITION OF THE CORNEAL IMAGE

let P be some point aperture in the focal plane of lens L_3. An image of the artificial pupil is formed in the focal plane on the opposite side of L_3, and any light from point P, or light in fact from any other point in the optical space, must pass through the confines of this image (i.e., the artificial pupil). The light from P is collimated by L_3 into a parallel beam labelled A′. If this beam impinges on a convex mirror (the cornea), then the virtual image of P is formed along the ray parallel to the beam A′ and passing through the center of curvature. As we have seen, the virtual image point, Q, is nominally half-way out on the radius. If we translate the light source from position A to some other position B, then the cone of light from P shifts and the collimated beam from L_3 shifts correspondingly, but the resulting beam B′ remains parallel to the original beam, and the virtual image position of P is therefore nominally the same--namely Q.

Thus, although lateral changes in the position of the light source shift the position of the artificial pupil formed on the cornea, and therefore shift the angle of the reflected rays, they do not affect the position of the virtual image in space.

Different tracking algorithms are possible besides the one shown in Fig. 19. For example, we could track one of the centers of curvature, in which case the returned rays from the corresponding mirror would not rotate in space at all, but then the rays from the other mirror would swing by approximately 2α for an eye rotation α. There could be advantage to stabilizing the returned rays from the very weak fourth Purkinje image, to ensure maximum intensity of that image. But other considerations might prevail to make the simple central tracking of Fig. 19 actually optimum. These other considerations relate to the magnitude of the image distortions with eye movement, and the limitations imposed by the real pupil on the fourth Purkinje image.

As far as image distortion is concerned, it is clear from Fig. 13 that the intercept angles would be smaller, and hence there would also be less distortion if the input beam was made to track the eye movement in the manner of Fig. 19. Thus, even to minimize effects due to image distortion there is an advantage in having the input aperture track the eye movement.

9. Limits Imposed by the Real Pupil

The real pupil of the eye can impose serious limits on the range of operation. To see this, assume that the input beamwidth 2W is equal to the pupil diameter D, and let us consider just the horizontal input beam represented by the extreme rays a and b in Fig. 21(a). This beam is reflected as rays a' and b'. (The parallel input beam is slightly converged as it passes the cornea, enough so to converge to a point on the cornea. But the retina is about 25 mm from the cornea, and the small amount of convergence does not significantly affect our qualitative arguments here.) As the eye rotates, some of the input beam is cut off. If the input beam had zero width (i.e., W = 0), an eye rotation

$$\alpha = \tan^{-1}\left(\frac{D/2}{a + \frac{r}{2}}\right) \qquad (15)$$

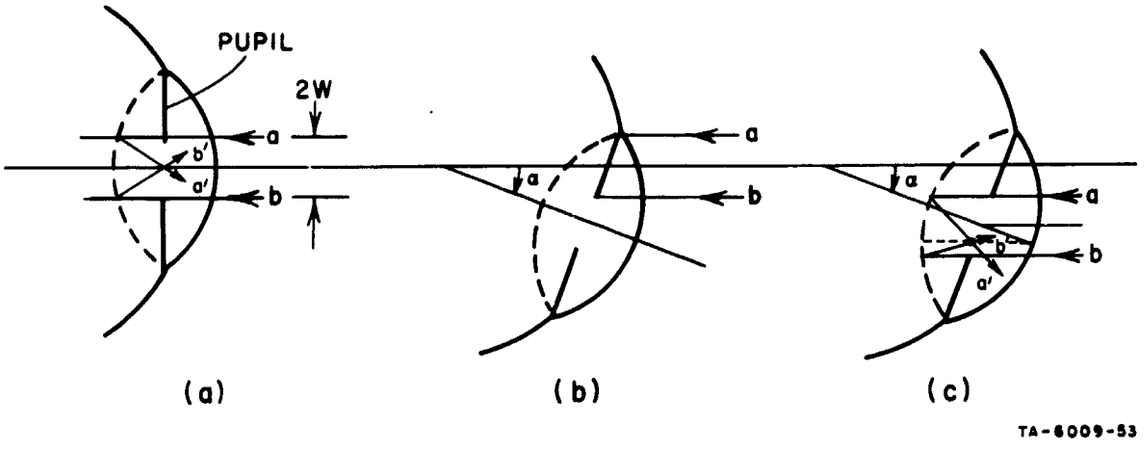

FIG. 21 EFFECT OF THE REAL PUPIL ON THE FOURTH PURKINJE IMAGE

(≈ 13 degrees for a 4-mm pupil) would cause the input beam to be completely cut off by the edge of the pupil. With the beam equal in diameter to the pupil, [Fig. 21(b)], as the eye rotates the light is cut off more gradually, in the manner of two equal-sized disks passing over each other, with the transmitted light being equal to the common area. The larger the input beam the larger the eye rotation needed to completely cut off the beam. In any case, we see from Fig. 21(c) that substantially full light is again transmitted if the input aperture is shifted in the direction of the eye movement.

The pupil can block not only input light but also reflected light. Recall that the fourth Purkinje image is a real image that falls almost in the plane of the real pupil. For the sake of argument let us assume that it falls exactly in the pupil plane, so that any part of the image that falls outside the pupil is completely blocked, or cut off from view. Movement of the artificial pupil does not have any first-order effect, since we noted that such movement has no effect on the position of the image formed in space. For example, in Fig. 22, if the input light in Beam a were not blocked by the pupil it would tend to form a real image at Point A, in the plane of the pupil. If we shift the artificial pupil so that the input beam is at a′, then none of the

input light is blocked, but still there is no output light because light focussing at A is blocked by the pupil.

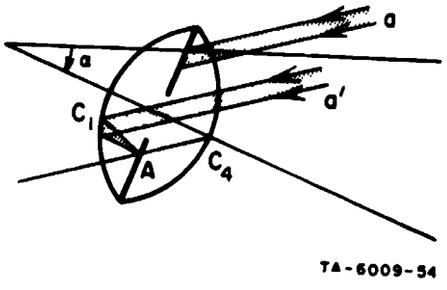

FIG. 22 LIMITATION BY THE PUPIL ON THE SIZE OF THE FOURTH PURKINJE IMAGE

Thus, we must be concerned with the pupil blocking output light as well as input light. Tracking with the artificial pupil can fairly well eliminate loss of input light. But as the eye rotates, the real image shifts in the pupil plane, and loss of portions of the image can set yet another limit on field of view.

We can readily determine the maximum angle of input light that will be blocked by the pupil after reflection by the back surface of the eye lens. The extreme condition is shown in Fig. 23(a) where parallel light at an angle θ is just cut off by the bottom edge of the pupil. The extreme input ray c passes through the center of curvature and reflects on itself

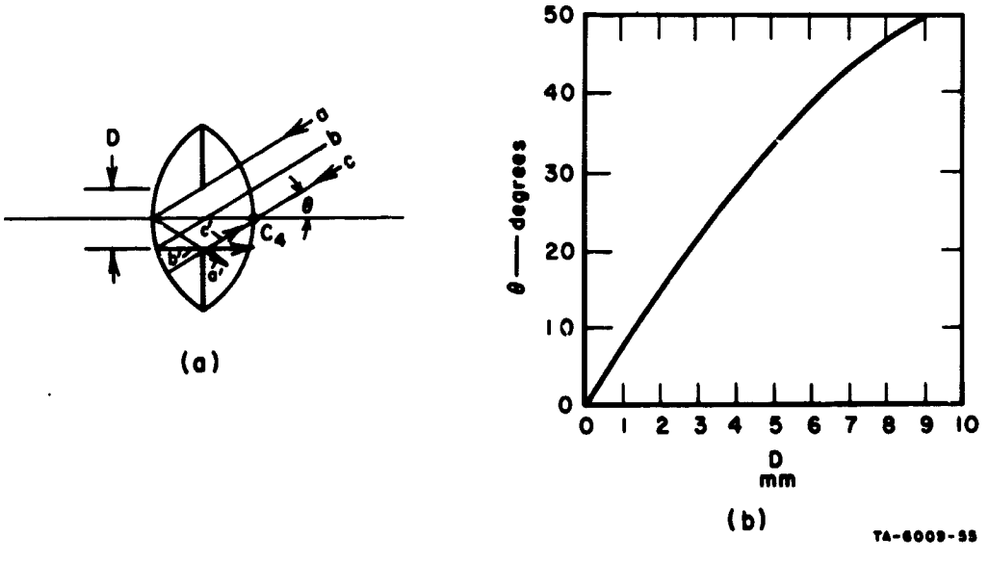

FIG. 23 CALCULATING THE MAXIMUM ANGULAR SIZE OF THE FOURTH PURKINJE IMAGE AS A FUNCTION OF PUPIL DIAMETER

as c′. The other extreme ray a is reflected as a′ and crosses c′ at the pupil edge. The central ray b, which is reflected as b′, does not quite cross c′ at exactly the same spot as a′, and is not blocked. Because of aberrations, in other words, the cut-off is not perfectly sharp, but the condition of Fig. 23(a) is a very good estimate of cut-off--namely,

$$\theta = \tan^{-1} \frac{D/2}{r/2} \qquad (16)$$

where D is the pupil diameter. This relation is sketched in Fig. 23(b). Thus, for a 4.5-mm pupil any light arriving at an angle greater than 30 degrees from the eye axis would be blocked by the pupil after reflection.

10. Optical Equalization of the Intensity of the Purkinje Images

Recall that the amount of light in the fourth Purkinje image is very much smaller than in the first Purkinje image--by a factor of 100 or more. This can impose severe dynamic range requirements on the electronic processing circuits. Some range compression can be achieved by nonlinear electronic amplification, but there is also an effective optical means of equalizing the image intensitites.

For a pinhole aperture stop ST_1 we saw in Fig. 14(b) that the light in the reflected image is collimated. Thus, for a line object, the reflected beam in space would similarly be a line, as indicated in Fig. 24(a) by the reflected rays a′, b′, c′ from corresponding points a, b, c, on the object. For an arbitrary aperture shape, the reflected beam (corresponding to each point of the line object) will have the same shape as the aperture, and the overall reflected beam in space will be the overlap of these beams, indicated in Fig. 24(b). In Fig. 18 we saw that the angular spread of the reflected beam is large, and, in fact, at the plane of the viewing lens the size of the overall beam will primarily be determined by the aperture stop. There will be a small spread, in the direction of the line object, which is nominally as large as the size of the line image in the eye. For our purposes here, let us assume that the total reflected beam simply has a cross-sectional shape equal to that of the stop.

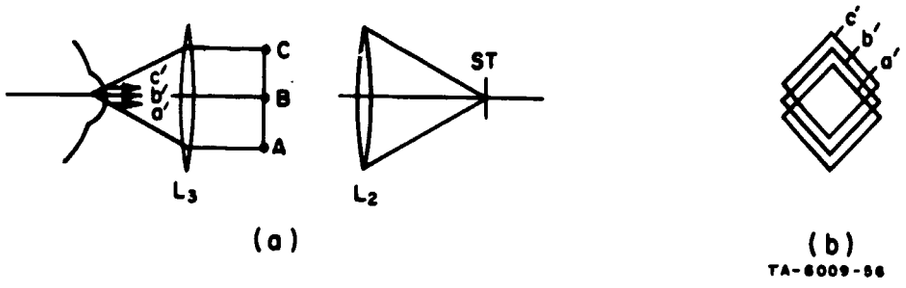

FIG. 24 DEMONSTRATION THAT THE OVERALL PATTERN OF REFLECTED LIGHT HAS ESSENTIALLY THE SAME SHAPE AS THE INPUT STOP ST_1

An important point with respect to the Purkinje images is that the reflected beams from the first and fourth images are inverted with respect to each other. For a triangular aperture stop, for example, the reflected beams in space will have the form shown in Fig. 25(a). With

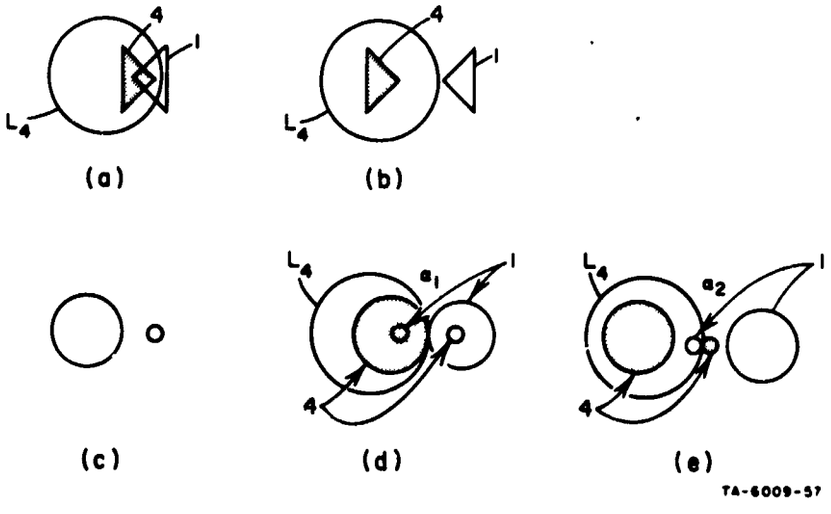

FIG. 25 RELATIVE MOVEMENT OF THE REFLECTED LIGHT BUNDLES, WITH RESPECT TO THE VIEWING LENS L_4
(a), (b) With a triangular stop ST_1 (c), (d), (e) With a double stop consisting of a large disk and a small satellite disk

the viewing lens L_4 placed as shown, a larger presentage of the light would be intercepted from the fourth than the first Purkinje reflection. As the eye rotates, the images separate, and for the case shown in Fig. 25(b) no light at all would be intercepted from the corneal reflection.

Of special interest is a stop consisting of a relatively large circular aperture and a small satellite aperture as in Fig. 25(c). In this case, the total light from each image is contained in two parts, a small circular patch of light and a large circular patch of light. At some particular eye position the large circular patches from the first and fourth images are tangent. In this condition, if the viewing lens is located as in Fig. 25(d), then the light in the large patch from the fourth reflection is intercepted, but only the light from the small patch of the first reflection. Thus, the percentage of total captured light from each image is in the ratio of the areas of the two disks in the aperture stop, assuming equal light intensity over the entire stop. Thus, for a 10:1 ratio in disk diameters, the total light intensity of the first Purkinje image can be reduced by a factor of $10^2 = 100$ compared with the total intensity of the four Purkinje image. This ratio of reduction is constant over an eye movement range from that shown in Fig. 25(d) to that shown in Fig. 25(e), beyond which we would rapidly lose the first image altogether.

This technique of optical equalization may be very important in the system design, at least in our first experimental model.

11. Two-Dimensional Tracking

Thus far we have considered only one-dimensional eye tracking--i.e., in a direction transverse to the other line. Recall from Sec. B-5 that the line images did not separate in space for an eye rotation parallel to the input line, but only for a rotation transverse to the line object. For tracking in two dimensions, the input pattern consists of a pair of orthogonal lines. If the input pattern is a pair of crossed lines, then the two images in space will similarly be a pair of crossed lines, as in Fig. 2, displaced according to the angular position of the eye. With a corresponding pair of scanning slits we obtain a measure of the separation of the corresponding lines in the two Purkinje images. With a series of scanning slits, as provided by the disk of Fig. 26, we can obtain a continual measure of the two-dimensional angular position of the eye. The task of the electronics is to measure the separation in the

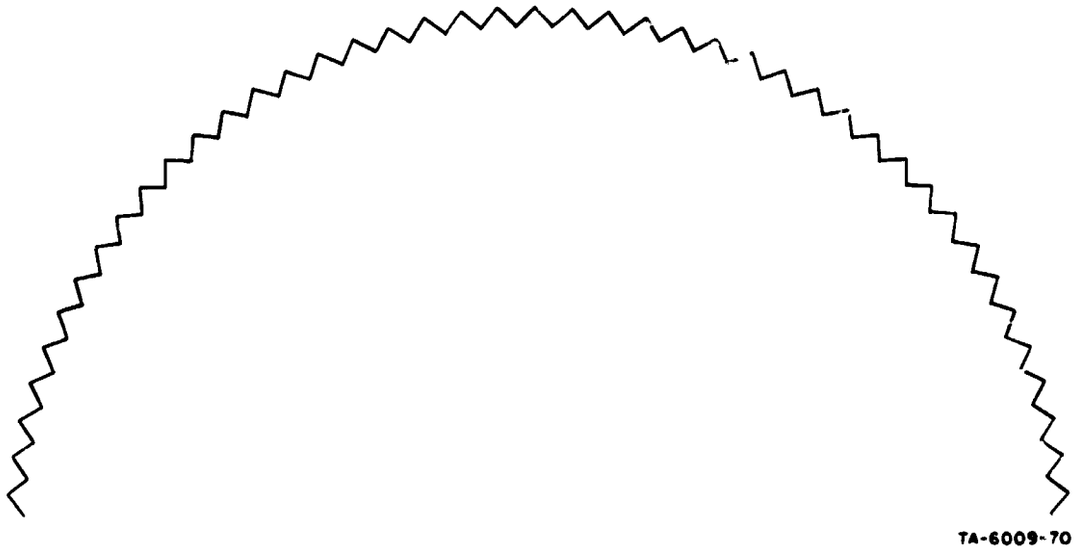

FIG. 26 PHOTOGRAPH OF A SECTION OF THE SCANNING DISK FOR CONTINUAL MEASURES OF x AND y POSITION

corresponding pair of peak signals in the photocell output, which provide a measure of eye position.

The scanning disk shown in Fig. 26, which will be used in the first experimental model, contains 180 alternately directed slits around the circumference. With the disk spinning at say 6000 rpm, or 100 rps, we obtain 9000 samples of x position and 9000 samples of y position per second. Actually, we only require about 100 samples of y position per second--i.e., a measure of eye position every 10 milliseconds or so--but the large number of samples allows us to achieve a good deal of averaging. This may be important because of the low level, and therefore noisy, signals involved.

BLANK PAGE

III INFRARED OPTOMETER

In this section we discuss a basic approach to the measurement of defocus and show how it is applied in the design of an optometer.

A. Measure of Defocus

Consider a bar of width W brought to focus at an image distance q, as in Fig. 27, and assume that the lens is completely covered except for

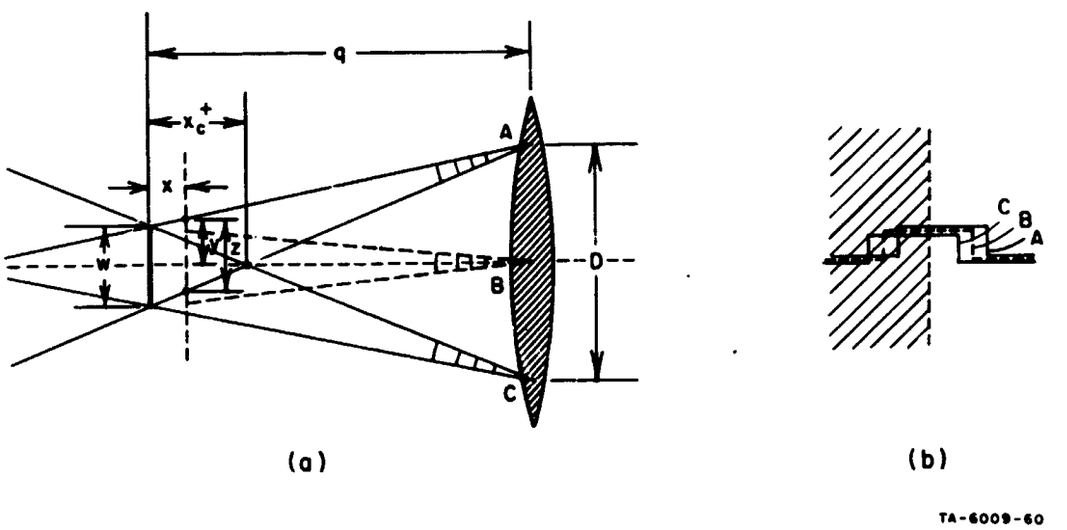

FIG. 27 FORMING AN IMAGE W THROUGH THREE PINHOLE APERTURES
(a) Three images overlapping in the image plane
(b) Images laterally displaced outside the image plane

three pinhole apertures A, B, and C. Let us consider the form of the defocus pattern at a distance x from the image plane. The light from each pinhole forms an in-focus version of the image in any plane, except that the images change size (being smaller with +x, and larger with -x), and shift laterally with respect to each other. We could determine both the magnitude and the polarity of defocus if we simply knew the amount of light intercepted from Apertures A, B, and C in one-half of the image, say to the right of the shaded region in Fig. 27(b).

Let L_A, L_B, and L_C be the total light intercepted from Apertures A, B, and C, respectively, in the right half of the image plane (assume that the left half of the image is completely blocked). We assume that the same total light passes through each aperture. For $x = 0$--i.e., in focus--we see that $L_A = L_B = L_C$. For $x > 0$, $L_A > L_C$, and for $x < 0$, $L_A < L_C$; the larger $|x|$, the larger $|L_A - L_C|$. Thus, by measuring $(L_A - L_C)$ we can determine both the magnitude and the polarity of defocus. The measurement of L_B provides no extra information and, in fact, L_B is independent of x. Thus, only two apertures are actually required and the larger their separation D the greater the sensitivity--i.e., the larger $|L_A - L_C|$ for a given $|x|$.

There exist critical values of x beyond which the magnitude of $L_A - L_C$ does not increase. For example, for $x \geq x_c^+$ in Fig. 27(a), $L_C = 0$ and L_A is equal to the total light passing through Aperature A. There also exists a negative critical value, x_c^-, such that for $x \leq x_c^-$, $L_A = 0$ and L_C is equal to the total light passing through Aperature C. A plot of $(L_A - L_C)$ as a function of x therefore has the form shown in Fig. 28.

Let us determine an expression for $(L_A - L_C)$ over the range $x_c^- \leq x \leq x_c^+$. From Fig. 27(a), we see that

$$L_A(x) = L\frac{y}{z} \tag{17}$$

when L is the total light from Aperature A, z is the beamwidth in plane x, and y is the intercepted part of z above the optical axis. The quantities y and z can be written as

$$y = \frac{W}{2} + \frac{x}{q}\left(\frac{D - W}{2}\right) \tag{18}$$

$$z = W\left(1 - \frac{x}{q}\right) \quad , \tag{19}$$

from which we find

$$L_A(x) = L\left[1/2 + \frac{D}{2W}\,\frac{1}{(q/x) - 1}\right] \quad . \tag{20}$$

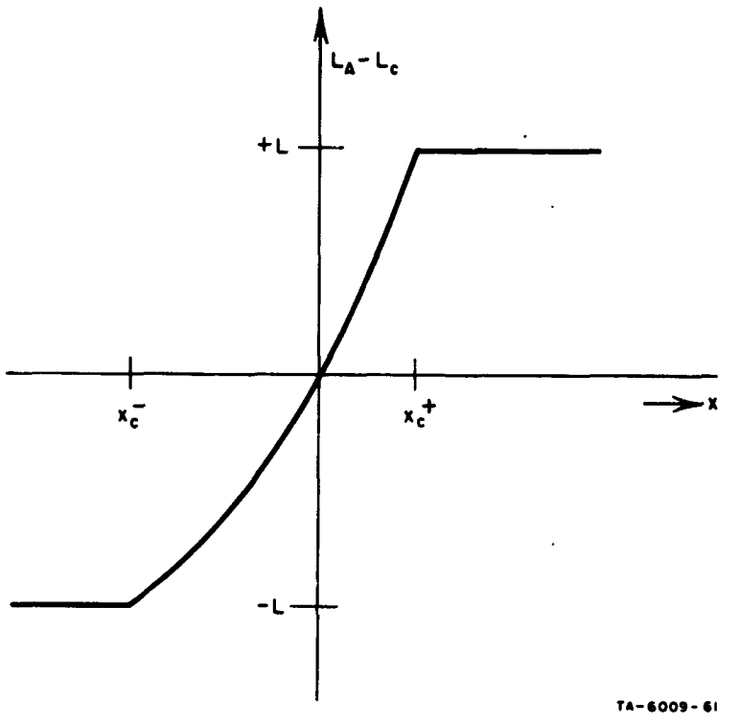

FIG. 28 PLOT OF THE DIFFERENCE IN LIGHT INTERCEPTED FROM APERTURES A AND C AS A FUNCTION OF THE DEFOCUS POSITION x

We can determine x_C^+--the plane in which the lower ray from Aperture A crosses the optic axis--by setting $L_A(x) = L$, from which we find

$$x_C^+ = q\left(\frac{W}{D + W}\right) \tag{21}$$

Assuming the same total light from Apertures A and C, then over the range $0 < x < x_C^+$ we have simply

$$L_C(x) = L - L_A(x)$$

$$= L\left[1/2 - \frac{D}{2W}\,\frac{1}{(q/x) - 1}\right] . \tag{22}$$

The difference signal $(L_A - L_C)$ is

$$L_A(x) - L_C(x) = \frac{DL}{W}\,\frac{1}{(q/x) - 1} \tag{23}$$

which is valid over the entire range $x_C^- < x < x_C^+$. The negative limit, x_C^-, is readily found to be

$$x_C^- = -q \frac{W}{D - W} \tag{24}$$

The plot of Fig. 28 is drawn for the case shown to scale in Fig. 27(a), namely D = 3W, in which case $|x_C^-| = 2|x_C^+|$. [Note that for $W \ll D$, $|x_C^+| \approx |x_C^-|$, and $(L_A - L_C)$ approaches a linear, symmetric function of x.]

Note that the function $L_A - L_C$ [Eq. (23)] is unaffected by lateral translation of the half-field stop in Fig. 27(b), except for shortening the range over which Eq. (23) applies, since with a lateral shift, L_A does not reach zero simultaneously with L_C reaching its maximum value, or vice versa.

Thus, we have all the information about defocus that we need if we simply determine L_A and L_C. If the light from Apertures A and C were distinctively different, then L_A and L_C could be measured simultaneously--e.g., if L_A and L_C were of different colors, or if L_A and L_C were orthogonally polarized, or if they were modulated at different frequencies. In any of these cases, the difference in outputs from two detectors would give us the required measure $(L_A - L_C)$. Only a single detector would be required, however, if it were properly time-shared. For example, suppose that the light from Apertures A and C had exactly the same properties but that the apertures were alternately opened and closed--the light passing through A, then C, then A, and so on. In this way, we would obtain sequential measures of L_A and L_C from only a single detector. If instead of only two discrete aperture positions, we moved a single aperture sinusoidally between extreme positions A and C, then the detector output would similarly be sinusoidal, which we can see from Eq. (20), where for a given value of x we replace the fixed term D by a sinusoidally varying term. In this case, the detector output is either in phase or 180 degrees out of phase with the mechanical movement, depending on the polarity of defocus x, and has a peak-to-peak amplitude $(L_A - L_C)$ given by the plot of Fig. 28, assuming a peak-to-peak mechanical swing D.

This is the basic measurement scheme used in the optometer--i.e., a single aperture is moved transverse to the optic axis in a sinusoidal fashion. In the actual instrument, however, a scanning light source is used instead of a scanning aperture, as we will describe in the next section.

B. Instrument Design

In this section we will outline some of the more important features of the optometer design.

1 Schematic of the Overall System Design

Figure 29 shows a sketch of the overall design of the optometer (Fig. 36 is a photograph of the actual instrument). We can think of the system as consisting of an input optical system and an output optical system. The input system--the horizontal portion at the top of Fig. 29--focuses an infrared bar pattern (formed by Stop S_1) onto the retina, and by servocontrol maintains the pattern in focus on the retina even though the refractive strength of the eye-lens may be continually changing. The input light projects through the beamsplitter in front of the eye. Reflected light from the retina that passes back out of the eye through the pupil is reflected downward by the same beamsplitter and imaged externally by the output optical system--the vertical portion at the left of Fig. 29. The image of the retinal pattern which is formed in Plane RI (for Retinal Image) falls on a stop, labeled S_2, which permits light from only half of the retinal image to pass to the detector—in the manner of Fig. 27(b). Before the light reaches the photoreceptor, however, that portion of light reflected from the cornea of the eye is blocked in Plane CI (for Corneal Image). A great deal of potential artifact signal is contained in the corneal reflection, so that blocking it is an extremely important step. The signal from the photodetector is then directed to a phase-sensitive detector, whose output is a dc signal with polarity and magnitude depending on the polarity and magnitude of the defocus. This signal in turn is used to drive the servomotor that controls the axial position of the bar pattern in the input system. In this way the bar pattern is maintained in focus on the retina.

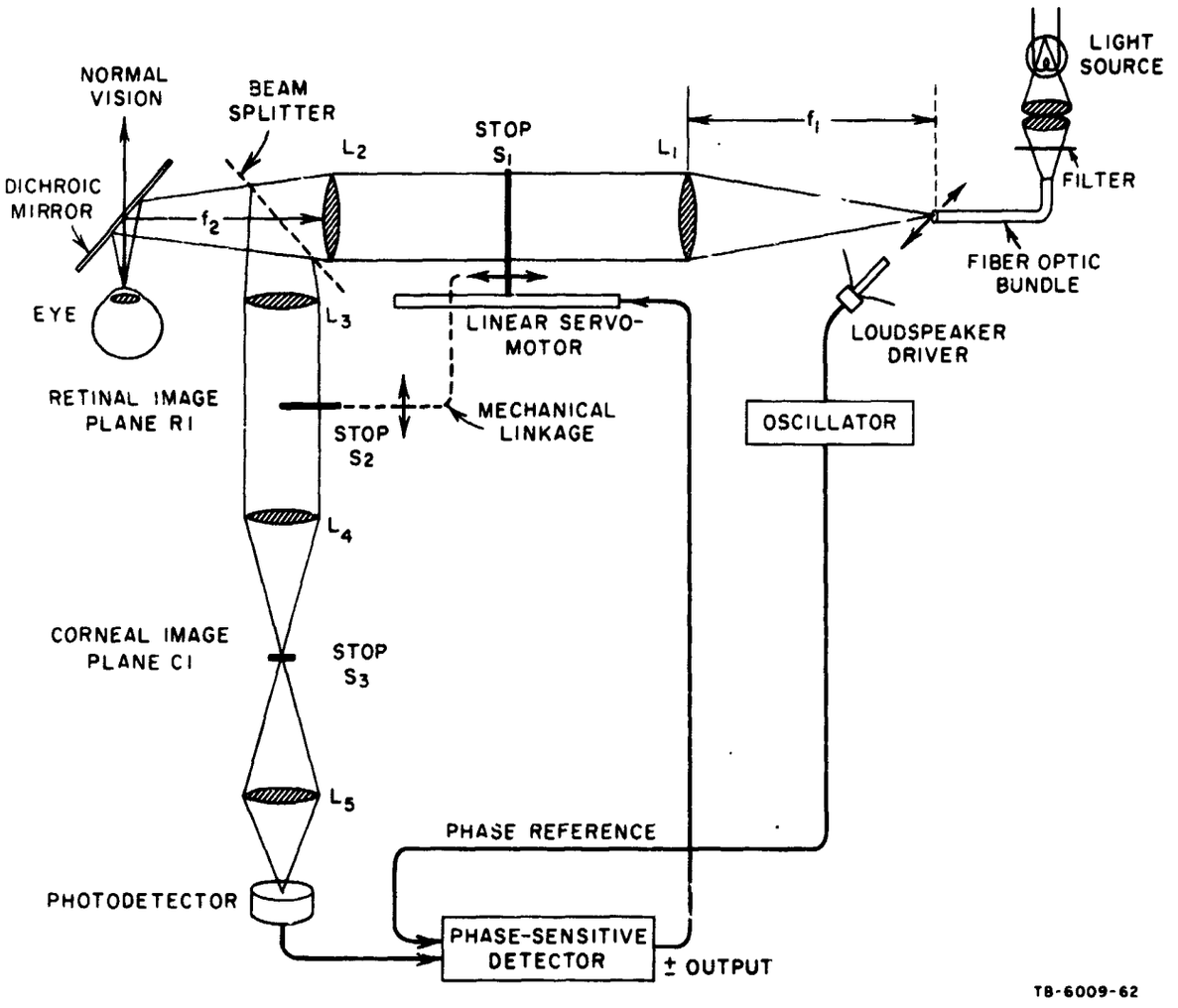

FIG. 29 SCHEMATIC DIAGRAM OF THE OPTOMETER

The servomotor also controls the axial position of Stop S_2 so as to maintain tne stop in the retinal image plane, in spite of changes in the refractive strength of the eye. Let us now consider the input and output system in more detail.

2. Input Optical System

The input system is shown in Fig. 30, with the eye symbolized simply by a lens L_E and a retina. The external lenses L_1 and L_2 project the pattern S_1 onto the eye, in effect through a double-aperture system, in the sense of Fig. 27(a). Let us consider the details of this projection.

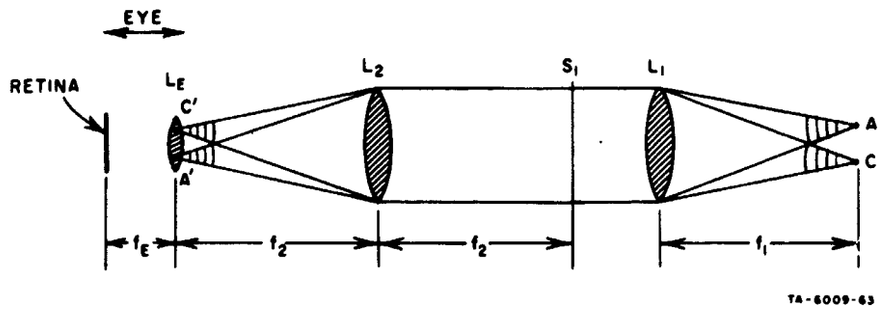

FIG. 30 INPUT OPTICAL SYSTEM, ASSUMING A POINT SOURCE OF LIGHT AT POSITIONS A OR C

Assume that a light source is placed at position A, in the focal plane of Lens L_1. Point A is then imaged in the focal plane of Lens L_2. The implication of this imaging is that any light from A that is intercepted by the two lenses must pass through the image point A', regardless of what sort of mask pattern may be placed between the two lenses. Similarly, if the light source is moved to position C, then all light from C that is intercepted by the optical system must pass through its image point C', in the focal plane of Lens L_2. In this way we have in fact created the condition implied in Fig. 27(a), but by a projection system rather than by the use of physical apertures placed at A' and C'. If the light source were moved continually between A and C, then the image of the light source would similarly move continuously between A' and C' respectively.

Let us next consider the introduction of the pattern S_1 that is to be focused onto the retina. To begin with, assume that the pattern is placed in the focal plane of Lens L_2, as shown in the figure. If we assume that the eye is accommodated for infinity, then this pattern will be in focus on the retina. In essence, L_2 and the eye-lens L_E form a double lens system, so that an object in the focal plane of one is automatically brought to focus in the focal plane of the other. But, of course, any light passing through the pattern S_1 must at any instant pass through the image of the light source. Thus, if the light source is at A then all light passing through S_1 must pass through the image point A'.

Thus far we have assumed that the light source is a point source. Let us now consider the use of an area source S, as in Fig. 31. The

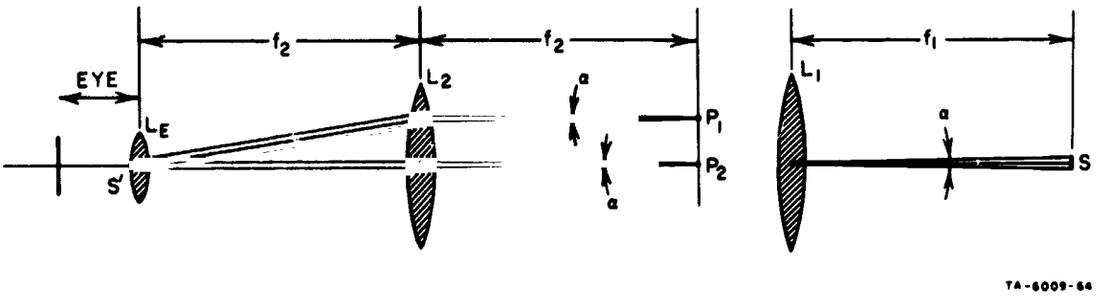

FIG. 31 IMAGE FORMATION WITH AN INPUT LIGHT SOURCE OF ANGULAR WIDTH α

light radiated from each point of the source is collimated by Lens L_1, so that to the left of Lens L_1 the collimated bundles have an angular spread α, where α is the angular size of the source as seen from Lens L_1. Thus the set of rays passing through a pinhole P_1 in S_1 have the same angular spread α. This bundle of rays emanating from P_1 is collimated by Lens L_2 to a width exactly equal to that of the source, assuming a unity magnification (i.e., $f_1 = f_2$), in which case $S' \equiv S$. Exactly the same arguments apply to any other point of the pattern, e.g., Point P_2 located on the optic axis. The bundle of rays from P_2 is also collimated by Lens L_2 into a parallel set of rays that exactly overlaps the collimated beam from P_1 in the plane of the pupil image S'.

Let us next consider the effect of moving the plane of the pattern along the optic axis, so that it is at a distance p from the lens L_2, where $p \leq f_2$, as shown in Fig. 32. The angular spread of the beam passing through P_1 is of course independent of the magnitude of p. However, for $p < f_2$ the lens does not collimate the bundle; rather, the refracted bundle appears to come from a virtual image point at a distance q behind the lens. An important point regarding this imaging technique is that the angular size of the image is independent of the distance p. This is readily deduced by noting that the locus of the horizontal ray through P_1 is completely independent of the distance p, and that the virtual image lies along the backward projection of this central ray.

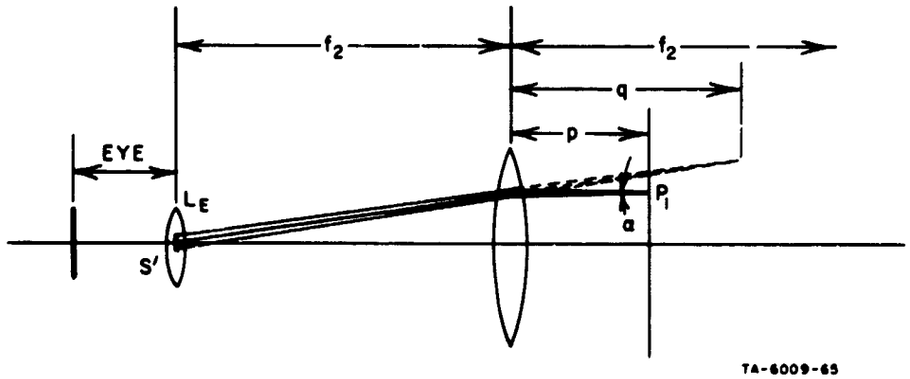

FIG. 32 CHANGE IN THE DISTANCE (f_2 + q) OF THE VIRTUAL IMAGE FROM THE EYE CAUSED BY CHANGING THE DISTANCE p — ANGULAR SIZE OF IMAGE REMAINS INVARIANT

Hence, by changing p we simply change the distance of the virtual image of the pattern but not the angular size of the pattern as seen from the eye.

Let us next consider the effective distance of the virtual image as a function of the distance p. Directly from the basic lens formula

$$\frac{1}{f} = \frac{1}{p} + \frac{1}{q} \tag{25}$$

we can write

$$q = \frac{f_2 p}{f_2 - p} \tag{26}$$

where the sign of q is reversed, since it is defined in Fig. 32 as being on the same side of the lens as p. The effective distance of the pattern image from the eye is then

$$(f_2 + q) = \frac{f_2^2}{f_2 - p} \quad . \tag{27}$$

In terms of dioptric distance from the eye, we can write

$$D = \frac{1}{f_2 + q} = \frac{1}{f_2}\left(1 - \frac{p}{f_2}\right) = D_o\left(1 - \frac{p}{f_2}\right) \qquad (28)$$

where D is the magnitude of accommodation required by the eye to focus the pattern which is located a distance p from Lens L_2, and D_o represents the accommodation required for p = 0 (i.e., with the pattern directly against the Lens L_2), in which case q = 0 and the pattern simply appears to be located at a distance f_2 from the eye, or at $D_o = 1/f_2$ diopters.

Thus, there is a simple linear relation between the distance p and the accommodation of the eye that maintains the pattern in focus on the retina. We can deduce the refractive power of the eye, as a continuous function of time, simply by recording p as a function of time, assuming that the input pattern is servo-controlled to maintain its retinal image continually in focus.

Let us now shift our attention to the output system, whose main function is to determine the state of focus of the retinal image and thereby control the input servo system.

3. Output Optical System

The optics of the output system are simple to follow if we assume that Lenses L_3 and L_4 (Fig. 33) are identical with Lenses L_1 and L_2, respectively, although this is by no means a requirement. By optical reciprocity it is clear that any light reflected from the retinal image would be reimaged at a distance p from Lens L_2, and therefore also at a distance p from Lens L_3. If the bar pattern is centered at the optic axis, then a stop S_2 in the retinal image plane will block half of the retinal image, in the sense discussed in connection with Fig. 27(b).

If it were not for blocking certain artifact signals we could put the photodetector directly behind this half-field retinal-image stop, and if the input light source were vibrated sinusoidally, orthogonally to the bar pattern, then we would obtain a sinusoidal output from the photodetector, of a phase and amplitude depending on the polarity and

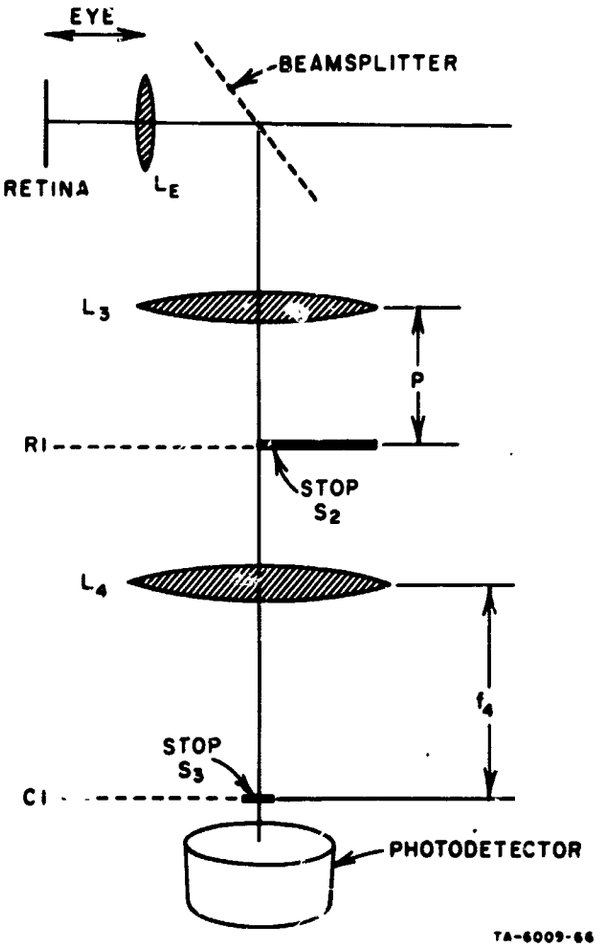

FIG. 33 OUTPUT OPTICAL SYSTEM

magnitude of defocus. However, a significant amount of light is reflected from the cornea, and as the light reflected from the cornea is modulated in space in response to the vibrating light source, significant artifact signal can be introduced into the photodetector at the same frequency as the desired signal.

We saw in Fig. 5(a) that the corneal image is formed almost exactly in the plane of the real pupil of the eye, which is the plane in which we image the light source or "artificial pupil" in Fig. 31. Thus, the corneal image will be reimaged in the focal plane of Lens L_4, which is optically equivalent to the plane of the original light source. We can prevent any light from the corneal image from entering the photodetector system by inserting a stop S_3 in the corneal image

plane CI. The stop must be at least as large as the corneal image itself and preferably larger, so as to be able to tolerate a certain amount of eye movements, which results in corresponding movements of the corneal image in space.

With the half-field stop in the retinal image plane, and with a corneal-image stop to eliminate the major source of artifact signals, we now have the potential for a relatively clean signal from the photodetector. This signal is fed to a phase-sensitive detector, as discussed in connection with Fig. 29, the output of which in turn controls the servo system.

Let us consider further the formation of the corneal image, and thereby obtain some idea of the size of the corneal stop that is required. It is undesirable to make the corneal stop any larger than necessary, because the stop blocks not only light from the corneal image but also a fraction of the useful signal light from the retina, which otherwise would pass through the entire pupil area. Two primary factors determine the size of the corneal stop: namely, the size of the corneal image itself and the tolerance necessary for eye movements.

Size of the Corneal Stop: We are concerned here with estimating the size of the corneal image and are not concerned therefore with the more complex considerations regarding image distortion treated in Sec. II. Assume that Stop S_1 consists of a bar of height h, as in Fig. 34, which has an angular size, as seen from the eye, of 2θ, where

$$2\theta = 2\tan^{-1}\left(\frac{h/2}{f_2}\right) \approx \frac{h}{f_2} \tag{29}$$

for small angles. For $p = f_2$--i.e., with the pattern located in the focal plane of Lens L_2--the corneal image is in the focal plane of the cornea and the image size h' is equal to the input pattern size scaled by the ratio of the focal lengths, or

$$h' = h\,\frac{r/2}{f_2} \tag{30}$$

where $r/2 \approx 4$ mm is the focal length of the cornea.

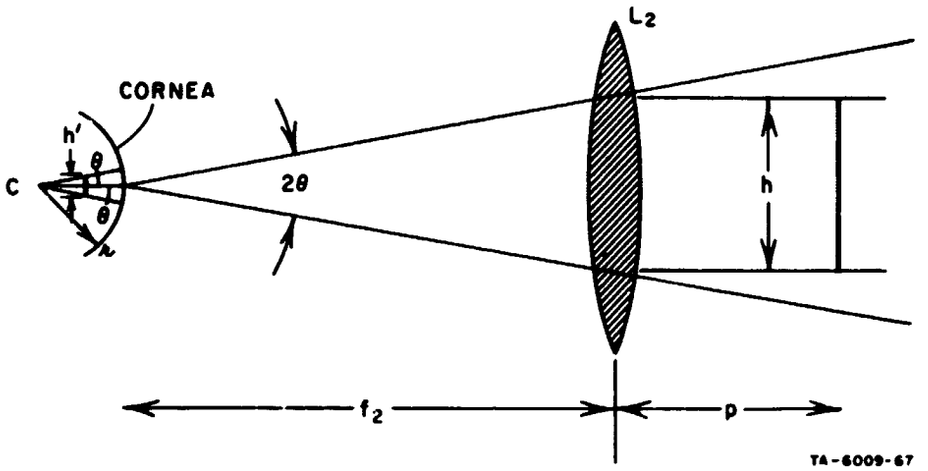

FIG. 34 ESTIMATING THE HEIGHT h' OF THE CORNEAL IMAGE, ASSUMING AN INPUT PATTERN OF HEIGHT h

We have already seen that the angular size of the image, as seen from the eye, is independent of p. This means that the locus of the end points of the corneal image is a pair of radial lines drawn through the center of curvature of the cornea, each at an angle θ from the axis, as shown in Fig. 34. As p decreases, the corneal image moves closer to the surface of the cornea and is correspondingly increased. To find the variation in image size we can again apply the basic lens formula and find that the image distance (measured from the surface of the mirror) is simply

$$q' = \frac{f_2(r/2)}{f_2 - (r/2)} = \frac{r}{2} \quad \frac{1}{1 - \frac{r/2}{f_2}} \tag{31}$$

so that we expect very little change in image distance for $f_2 \gg r/2$, which will generally be the case. For example, for $f_2 = 85$ millimeters, then $(r/2)/f_2 \approx 1/20$, and there is only a 5-percent change in the image distance over the entire range $0 \leq p \leq f_2$. Thus, for all practical purposes we can consider the corneal image to be permanently fixed in the r/2 plane and to have an image of the size given by Eq. (30).

If we assume that under the conditions of use the pupil will not stop down less than, say, 4 mm, then we may wish to confine the

height of the bar in the corneal image to only 1 mm, in which case $h \approx 22$ mm (assuming a focal length again of $f_2 = 85$ mm, which corresponds to an angular size $2\theta \approx 15$ degrees.

To find how the corneal image moves in space in response to an eye movement, it is only necessary to know how the center of curvature of the cornea moves. The key dimension is the distance from the center of curvature of the cornea, C, to the center of rotation of the eye, CR, which Fig. 3 shows to be ≈ 6 mm. For small movements we have that

$$m \approx a\alpha \tag{32}$$

where m is the lateral movement of the corneal image in response to an eye rotation α. For eye movements over, say, a 5 degree field, the corneal image will thus move by approximately $m \approx \pm 0.25$ mm. To allow for eye movements of this size we must then enlarge the corneal stop by about 0.5 mm in every dimension, beyond the size determined strictly on the basis of the size of the corneal image itself.

4. Physical Design of the Instrument

A schematic drawing of the instrument is shown in Fig. 35 and a photograph in Fig. 36. In order to avoid a bulky instrument that extends in two orthogonal directions, the optics have been folded so that the input and output paths are parallel and separated by a distance d = 20 mm, which is an extra distance that the input path light has to travel in the reflection from the dichroic mirror to the beam splitter. The two output lenses and Stop S_1 are axially displaced from the input lenses and Stop S_2 by this same distance, so that they are in optically equivalent planes. The stops are mechanically coupled and are driven by a single servomotor.

Lenses L_1, L_2, L_3, and L_4 are identical achromatic doublets, with an 85 mm focal length and 25 mm diameter. With identical lenses, there is unity magnification in the input and output optical systems.

The fiber-optic bundle is 12 inches long and has an effective end area of about 1.0 mm. It is illuminated at one end by a 45-watt

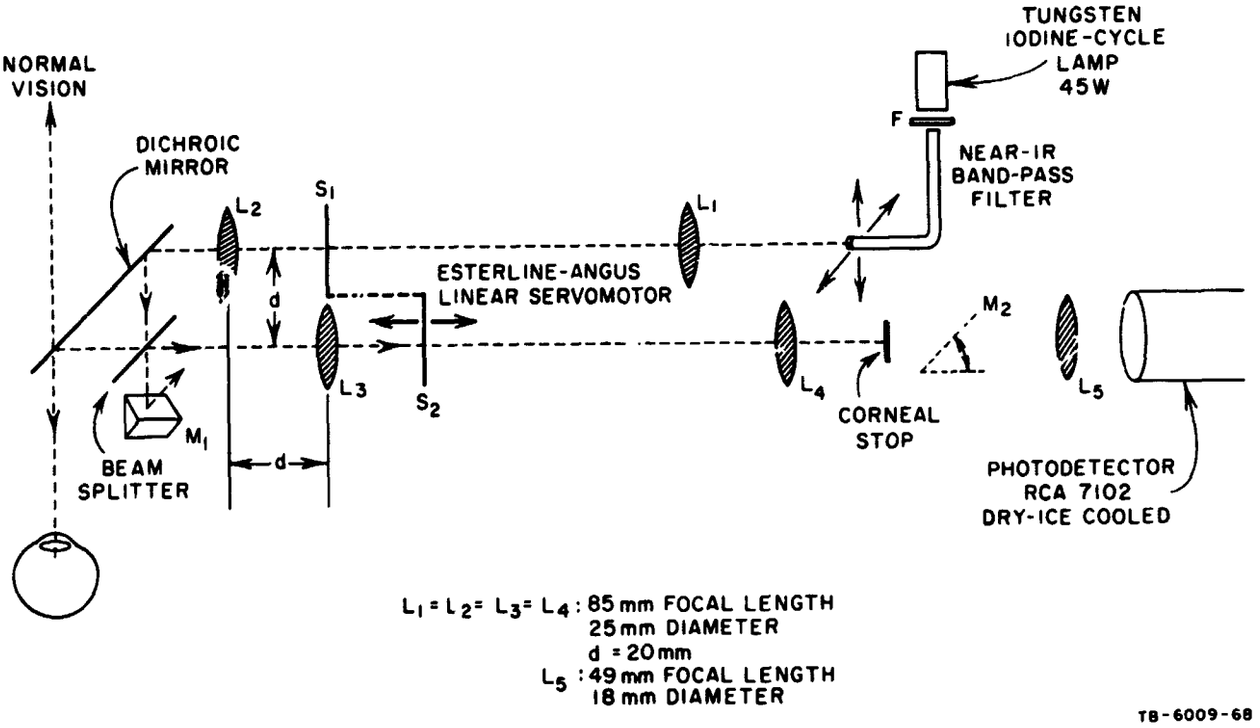

FIG. 35 DIAGRAM OF THE OPTICS OF THE ACTUAL INSTRUMENT

high-intensity bulb mounted in a conventional optical condenser system. The other end of the fiber-optic bundle is mounted in a two-dimensional vibrator, controlled by two orthogonally mounted loudspeakers whose cones have been removed. Although vibration in only a single dimension is required for optometer purposes, this instrument also offers the possibility of measuring astigmatism. This can be accomplished by rotating the bar pattern in which case we must similarly rotate the direction of the light-source vibration. The orthogonal drive system permits us to vibrate the fiber-optic bundle in any desired direction.

Mirror M_1 reflects the undesired component of the input light out of the system. Lens L_5 images the final signal light onto the photodetector. The corneal stop is mounted in a clamp which provides fine position control in three orthogonal directions. A rotatable mirror M_2 permits direct viewing of the optical output without having to move the photodetector. In normal operation the mirror is lowered out of the way.

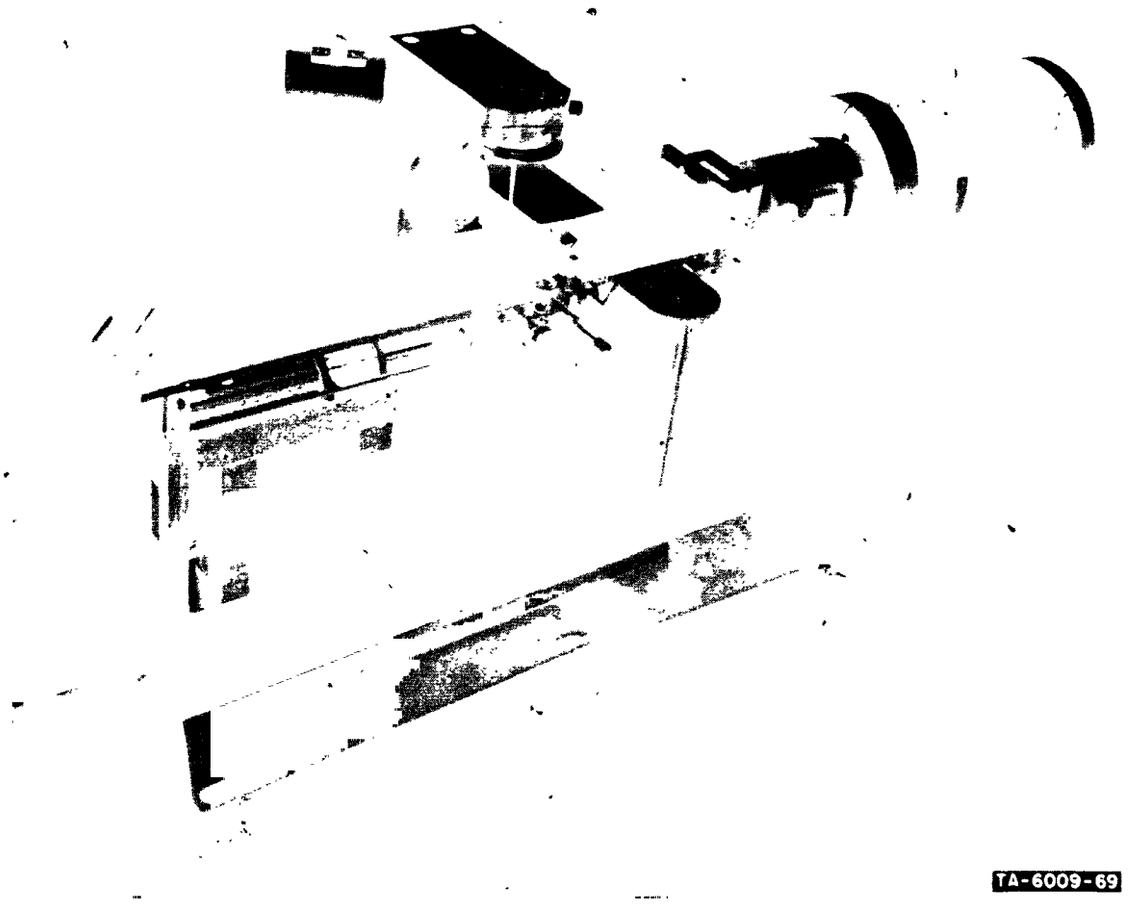

FIG. 36 PHOTOGRAPH OF THE OPTOMETER

IV STATUS OF THE EYE TRACKER AND OPTOMETER

Signals in the form of Fig. 2 have been obtained from an experimental version of the eye tracker, with human subjects, using the optical equalization method discussed in connection with Fig. 25. These signals seemed to respond appropriately to eye movements. Electronic circuits to process these signals are now being tested. Without automatic signal processing it is difficult to evaluate the sensitivity and accuracy that may be achieved. The signals are noisy and of relatively low amplitude, and some new optical configurations to help increase the optical efficiency of the system are now being examined. We hope shortly to decide on an optimum configuration.

We have not yet been able to completely test the optometer, since the servo-drive system and properly coated dichroic and beamsplitter elements are just now being incorporated into the system. The unit seemed to function properly, however, with a model eye and some available optical elements (without proper coatings), and with Stops S_1 and S_2 operated manually. We hope to test the complete system, with human subjects, very shortly.

REFERENCES

1. H. D. Crane, "A Theoretical Analysis of the Visual Accommodation System in Humans," Final Report, Contract NAS2-2760, SRI Project 5454, Stanford Research Institute, Menlo Park, California (January 1966).

2. F. W. Campbell and J. G. Robinson, "High-Speed Infrared Optometer," J. Opt. Soc. Am., Vol. 49, No. 3, pp. 268-272 (March 1959).

3. J. Warshawsky, "High-Resolution Optometer for the Continuous Measurement of Accommodation," J. Opt. Soc. Am., Vol. 54, No. 3, pp. 375-379 (March 1964).

4. H. Davson, ed., The Eye, Vol. 4, Table II, p. 111 (Academic Press, New York, N. Y., 1962).